Palestine Polytechnic University

Deanship of Graduate Studies and Scientific Research

Master of Civil Engineering

Flexural Performance of RC Beams Strengthened with Longitudinal SMA

Done by:
Mohammad Ahmad Makhtoub

Supervisor:
Ph.D. Belal ALmassry

Thesis submitted in partial fulfillment of requirements of the degree
Master of Civil Engineering

July, 2023

The undersigned hereby certify that they have read, examined and recommended to the Deanship of Graduate Studies and Scientific Research at Palestine Polytechnic University:

Flexural Performance of RC Beams Strengthened with Longitudinal SMA

Mohammad Ahmad Makhtoub

in partial fulfillment of the requirements for the degree of Master in Civil Engineering.

Graduate Advisory Committee:

Prof./Dr. …… University: ……

Signature:———————————— Date:————————————

Prof./Dr. …… University: ……
Signature:———————————— Date:————————————

Prof./Dr. …… University: ……
Signature:———————————— Date:————————————

Prof./Dr. …… University: ……
Signature:———————————— Date:————————————

Thesis Approved by:

Name:

Dean of Graduate Studies & Scientific Research

Palestine Polytechnic University

Signature: …….

Date: …….

Flexural Performance of RC Beams Strengthened with Longitudinal SMA

Mohammad Ahmad Makhtoub

Abstract

Nowadays, new materials have appeared that have played an important role to improve the structural behavior of RC members. the flexural performance of shape memory alloys (SMA) of RC beams will be studied. Many specimens with different parameters with longitudinal rebars of SMA and the other without SMA will be presented, and the specimens will be analyzed using programs that based on Finite Element Method (FEM) such as Abaqus program.

A parametric study will be conducted using the following parameters: the diameter of rebars, and the distance between the loads on flexural strengthening for RC beams by using longitudinal rebar of SMA and steel, the results will be compared to experimental literature, additionally, the relationship between loads and displacement for RC beams will be drawn, as well as the relation between ductility and flexural strengthening.

تعزيز أداء الإنحناء للجسور الخرسانية المسلحة باستخدام قضبان ذاكرة الشكل

محمد أحمد مخطوب

المستخلص

في الوقت الحاضر، ظهرت مواد جديدة لعبت دورًا مهمًا في تحسين السلوك الهيكلي العناصر الانشائية المسلحة. سيتم دراسة أداء الانحناء لسبائك ذاكرة الشكل (SMA) لعزم الجسور المسلحة. سيتم تقديم العديد من العينات ذات المحددات المختلفة مع حديد التسليح الطولي لـ سبائك ذاكرة الشكل والأخرى بدون سبائك ذاكرة الشكل، وسيتم تحليل العينات باستخدام البرامج التي تعتمد على طريقة العناصر المحدودة (FEM) مثل برنامجAbaqus.

سيتم إجراء دراسة باستخدام المحددات التالية: قطر حديد التسليح، والمسافة بين الأحمال على تقوية العزم للجسور الخرسانية المسلحة باستخدام حديد التسليح الطولي من سبائك ذاكرة الشكل والحديد، وستتم مقارنة النتائج بالدراسات التجريبية، بالإضافة إلى العلاقة بين الأحمال والإزاحةوالمرونة والعزم للجسور المسلحة.

Dedication

Praise be to Allah, Lord of the worlds

To the Prophet Mohammad

Blessings and Peace be upon him

To my father

To my mother

To my brother

To my sisters

To my precious ones

To all friends and colleagues

To my teachers

To everyone working in this field

To all of them

I literally dedicate this work

Acknowledgment

First of all, praise is to Allah for helping me in making this research possible. I would like to extend thanks to many people who helped me during my research work. Countless words are to be said in acknowledging the efforts of my enthusiastic supervisors – Dr. Belal ALmassry. Their tremendous academic support and continuous
encouragement cannot be shortened in few words.
Special thanks to Dr. **Belal ALmassry** from the civil engineering Department. Many thanks to the defense committee for their efforts in reviewing my thesis.
Special gratitude is to the Computer Engineering Department for providing

Special mention goes to my parents, brothers, sister, friends and colleagues.

الإقرار

أنا الموقع أدناه مقدم الرسالة التي تحمل عنوان:

Flexural Performance of RC Beams Strengthened with Longitudinal SMA

أقر بأن ما اشتملت عليه هذه الرسالة إنما هي نتاج جهدي الخاص، باستثناء ما تم الإشارة اليه حيثما ورد، وأن هذه الرسالة ككل، أو أي جزء منها لم يقدم لنيل أي درجة أو لقب علمي أو بحثي لدى أي مؤسسة تعليمية أو بحثية أخرى

Declaration

I declare that the Master Thesis entitled ”Flexural Performance of RC Beams Strengthened Using SMA Bars” is my own original work, and herby certify that unless stated, all work contained within this thesis is my own independent research and has not been submitted for the award of any other degree at any institution, except where due acknowledgement is made in the text.

Student Name: Mohammad Ahmad Makhtoub

Signature:———————————— Date:————————————

Table of Contents

List of Figures

List of Tables

Chapter 1: Introduction

Nowadays, new materials have appeared that have played an important role to improve the structural behavior of RC members. the flexural performance of shape memory alloys (SMA) of RC beams will be studied. Many specimens with different parameters with longitudinal rebars of SMA and the other without SMA will be presented, and the specimens will be analyzed using programs that based on Finite Element Method (FEM) such as Abaqus program.

A parametric study will be conducted using the following parameters: the diameter of rebars, concrete compressive strength, yield strength of steel on flexural strengthening for RC beams by using longitudinal rebar of SMA and steel, the results will be compared to experimental literature, additionally, the relationship between loads and displacement for RC beams will be drawn, as well as the relation between ductility and flexural strengthening.

1.1 Overview

Improving the flexural performance of RC beams hasbecome an essential issue for engineers, A shape-memory alloy is one that can be deformed when cold and then return to its original shape when heated. SMA rebars are commonly made from copper-Aluminium-Nickel-based and Nickel-Titanium-based alloys.

Several types of studies on the behavior of RC members reinforced with SMA rebars have been done during the past ten years.(Pereiro-Barceló et al., 2018), Additionally, the finite element technique (FEM) was used, and the numerical results and experimental results were compared. Results of this study showed that utilizing SMA reinforcement greatly increases the ductility of the RC beam without reducing its bearing capacity.

A new model to predict the flexural behavior of SMA RC beams based on Timoshenko theory was proposed after research into the flexural performance of RC beams reinforced with many circular SMA rebars.The results demonstrated that when the temperature

increased close to the final austenitic temperature, the bending behavior of SMA RC beams was significantly improved. (Viet and Zaki, 2019).

1.2 Definition of ductility

Ductility describes the capacity of a terial/section/member/structure to undergo large deformations without any significant reduction in strength.There are, however, many levels of ductility, such as material ductility, section ductility, member ductility, and structural ductility. Material ductility, as indicated by standard stress-strain curves, has a fundamental level of ductility that represents the maximum ductility if all points of structure have the same behavior and are strained equally, which is extremely unlikely. Sectional ductility is lower than material ductility because the sections' layers of materials are not uniformly strained. Member ductility is much lower than sectional ductility because the member often yields only at certain locations. Finally, structural ductility is the lowest since every structure has multiple members that do not all reach plastic capacity at the same moment.

Generally, ductility of a structure is affected mostly by joint failures(Ghobarah and Said, 2002). Thus, ensuring sufficient ductility at the joints can increase overall structural ductility.

1.3 Scope of research

Nowadays, developing the science of using modern materials plays a vital role to improve the structural behaviour of concrete members. This study aims to compare the influence of shape memory alloys (SMA) and steel longitudinal rebars on both flexural performance of reinforced concrete (RC) beams. The research will focus on the effect of shape memory alloys (SMA) on flexural strengthening of RC beams, it will be based on three parameters concrete compressive strength, the diameter of rebar and yield strength of steel:

A FE numerical model using the commercial software Abaqus will be conducted, the non-linear behavior of materials will be taken into account, the numerical model will be

validated using previous experimental results which tested the performance of RC beams strengthened using SMA rebars.

The model will then be used to conduct a parametric study, throughout changing one parameter and fixing others, then the results will be compared in order to study the effect of parameters on flexural strengthening of RC beams, the results will be compared to other practical experiments using scientific papers of researchers who have studied the same topic in the same practical.

The RC beams strengthened with SMA will be compared to other RC beam strengthened using GFRP, a special investigation will be paid to the modes of failure for those beams, a hybrid strengthening technique will be proposed.

1.4 Research objectives

The main objective of this study is to quantify the effect of using certainrebars of SMA in R.C Beam to improve flexural before failure.To achieve this prime goal, the following tasks are performed:

1- Study literature on using SMA rebars in RC beams . This will be elaborated in Chapter 2.
2- Develop a 3-D non-linear F.E. model for R.C beam. The model includes both material and geometrical nonlinearities, and includes interfacial properties between SMA and concrete. The commercial (F.E.) software ABAQUS is used to create a generic parametric model of R.C beam with and without SMA rebars. Geometry, materials, and all the required input data are obtained from the literature and used to develop the model.
3- Verify the model by comparison with published experimental data. Sensitivity and parametric studies in order to identify the important and significant parameters that influence the ductility of the beam. This is presented in Chapter 4 of the thesis.

4- Correlate the results obtained from the F.E. models. This is shown in Chapter 5.
5- Verify the results by comparing numerical results with analytical results using basics of mechanics and plasticity. This is shown in details in Chapter 6.
6- Summarize the results and draw conclusions and recommendations for engineers on the use of SMA and future works.

1.5 Research methodology

Due to its low cost, speedy results, and capacity for in-depth research on numerous variables, numerical analysis of structures offers an appealing method of research. As a result, the commercial software ABAQUS is used to create a three-dimensional non-linear F.E. a simply supported beam model. The general description of a R.C. simply supported beam modeling is illustrated in this chapter, while the material parameters for this model are shown in the chapters on verification and parametric study. The following subsections will explain various aspects of modeling the beam, including material description, part generation, interface modeling, analytic regime selection, loading setup, boundary conditions, and meshes.

1.6 Research hypothesis

The following parameters, which were taken into consideration when performing this study and are based on preceding data from the literature review and are believed to have no bearing on the results:

- The reinforcement (steel and SMA) was determined to be completely attached to concrete with no sliding by accounting for the required development length and feeding the reinforcement through the support points. Additionally, embedded region restrictions were used to represent all reinforcing components.
- The bottom of the beam was supported by two steel plates, one of which served as a roller and the other as a pin support. Two top steel plates were fastened in order to distribute the load to the beam. In this instance, the four-point load test approach is applied.

- Static loads were used to study the outcomes without taking into account the effects of dynamic loads.
- For the transfer of the load supplied to steel plates to beams, beams are fully fastened to steel plates.
- The stress placed on the beams was statically growing.

Chapter 2: Literature Review

2.1 Introduction to Shape memory alloys

metallic alloys that have the ability to recover their original shape after undergoing large deformations, when the temperature is increased specific level, (Gibert, 2019).

One day in 1959, while Buehler done studies about NiTi alloy variation percentage of the two components in order to checks the material properties, he observed different sounds produced from the small bars of NiTi alloy used for the experimental tests, if were free to fall down, according to their temperature, so he concluded different damping properties and they had different atomic arrangements, in addition, it was possible to induce a variation in this behaviour simply heating or cooling the small bars, ("Granito_Michele_23.pdf," 2010.).

since the discovery of the shape memory effect (SME) in Ni-Ti alloys in 1963, many research has done on different systems of SMAs to study their properties.(Hsu, 2013.)

Today the studied shape memory alloys usually are Nickel-Titanium, Copper-Zinc-Aluminumand Copper-Aluminum-Nickel that used to produce SMA rebars (Karimipour and Edalati, 2020).

Table 1: Some S.M.A. property("Granito_Michele_23.pdf," 2010.)

Properties	Ni-Ti	Cu-Zn-Al	Cu-Al-Ni
Max Temp. shape recovery (°C)	100	120	200
Max recoverable deformation (%)	8	6	5
hysteresis (°C)	12-50	10-25	15-20
Austenitic yield stress (MPa)	415	350	400
Martensitic yield stress (MPa)	70	80	130
Stress rupture (MPa)	700	600	500-800
Density (g/cm3)	6.5	7.6-8.0	7.2
Resistivity (microohm-cm)	80-90	8.5-9.7	11-13
Thermal capacity (J/Kg °K)	837	400	373-574
Thermal conductivity (J/m*sec*°K)	18	120	30-43

2.2Shape Memory Alloys (SMAs) applications:

In the last years in particular, high-quality features, reduced production costs and availability of materials allowed development of several products in many fields aerospace, civil, mechanic, medical and other("Granito_Michele_23.pdf," 2010.).

The properties in civil structures summarizing as:

1- The large force produced as a result of returning to its original shape.
2- huge amounts of strain energy are repeatedly absorbed while being loaded without permanent deformation.
3- perfect damping properties at temperature below the transition range.
4- perfect characteristics of corrosion resistance and non-magnetic in nature.
5- Under large strain cycles, low density and high resistance.
6- The ability to be electrically heated for shape recovery (Dolce and Cardone, 2001).
7- The protecting of cultural treasures and old structures was Among the earliest uses of SMA in civil structures(Dolce and Cardone, 2001).

2.3Ni-Ti-Nb ALLOYS IN STRUCTURAL ENGINEERING

The addition of (Nb) to a binary alloy (Ni-Ti) affects and widen the thermal hysteresis and make these ternary alloys useful for prestressing applications in civil engineering.They have larger temperature hysteresis. This allows the material to be prestrained at a low temperature phase called martensite be safely transported at ambient temperatures, be activated at a higher temperature with reverse transformation to austenite (high temperature phase) and retain high values of recovery stresses at ambient temperatures.

Analyzed the various recovery stress generating ranges binary Ni-Ti and ternary Ni-Ti-Nb are two distinct alloys. It is shown schematically in 2.1, 2.2, and 2.10 are figures. A stress-strain path for a narrow hysteresis alloy is shown in Figures 2.1 and 2.2 (i.e., Ni-Ti), as well as Figures 2.1b and 2.2b, a wide hysteresis alloy (i.e. Ni–Ti– Nb)

In these cases, the process starts with a pre-treatment with loading and the material being twinned martensite, evolving with an almost horizontal plateau, in which the detwinning process takes place and unloading with a pre-strain maintained. For Ni–Ti alloys, in case of impeded strains, the recovery stress increases during heating but decreases during subsequent cooling (fig. 2.1a and 2.2a). (Cladera et al., 2014)

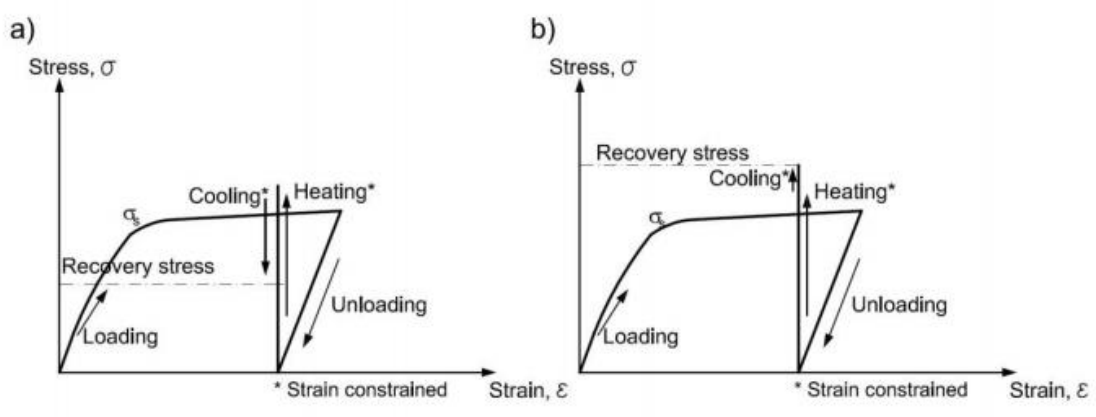

Figure 1: Schematic stress–strain diagrams of pre-straining and generation of recovery stresses during the activation of the reverse transformation in a constrained SMA: a)Narrow hysteresis alloy, i.e., Ni–Ti; b)wide hysteresis alloy, i.e., Ni–Ti–Nb. From (Cladera et al., 2014)

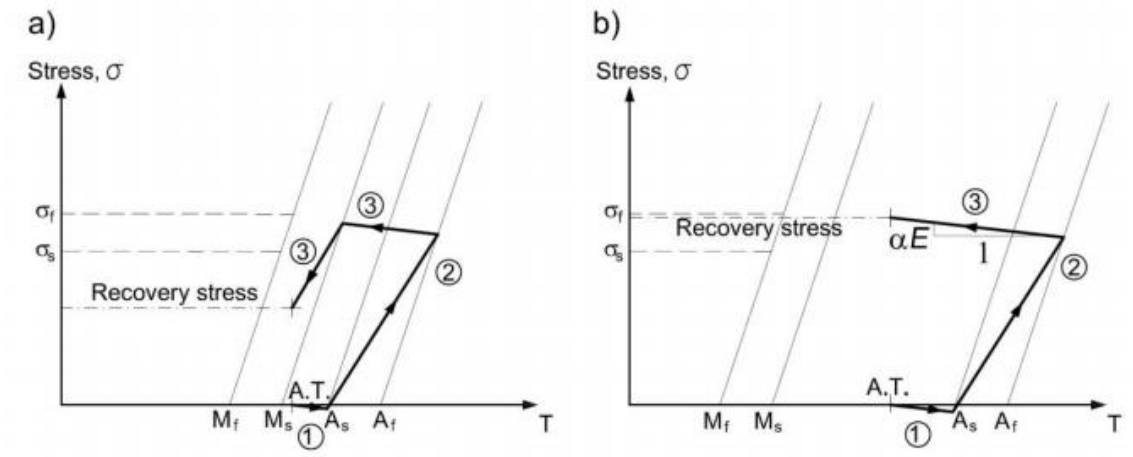

Figure 2: The evolution of recovery stresses and temperature during heating and cooling of the two a) narrow hysteresis alloy, i.e., Ni–Ti; b) wide hysteresis alloy, i.e., Ni–Ti–Nb. From (Cladera et al., 2014)

The previous figure shows the temperature and recovery stresses of the two alloys stated above when they are heated and cooled. . The elastic stress decreases in the heating step (path 1). Due of the suppressed thermal expansion, A reverse change to the austenite phase occurs once the stress temperature path passes the As boundary (path 2) Due to the inhibition of contraction caused by this transition, the SME is activated, producing tensile stresses in the SMA until the alloy is completely transformed into austenite. However, some of the stress is lost due to thermal expansion. The thermal expansion effect is

recovered by thermal contraction during subsequent cooling (Lee et al., 2013).Using Eqs, it is possible to determine the slope of the stress variation due.

2.4 Active Strengthening of Reinforced Concrete Beams Using Shape Memory Alloys

2.4.1 Prestressing through SMA wires

A well-known and widely developed technique to enhance the mechanical behavior of Prestressing RC structures (Maji and Negret, 1998) carried out one of the earliest research experiments in which Ni-Ti wires were employed to create an additional prestressing force to cement mortar elements. In the martensite phase, the cables were pre-strained beyond their elastic limit and then embedded in the beams. through electrical warming the transformation from martensite to austenite created recovery stresses in the SMA as well as compressive stresses in the mortar.

Despite the fact that the adherence of SMA wires to concrete has been a major technological concern, (Czaderski et al., 2006)

SMA prestressing of RC structures has the advantage of not requiring hydraulic jacks and can be used at any time during an element's lifetime.

These outcomes new possibilities, such as prestressing in stages to avoid cracking. Furthermore, there are no friction losses; this could be especially useful when the prestressing layout is particularly curved, (Janke, 2005).

Improvement in wire bonding was studied in 2006, Although the chlorides in the resin caused unacceptable corrosion problems in the SMA, epoxy resins were used to fix quartz sand on the surface of the wires.(Deng et al., 2006) used prestressing to produce counter-deflections in small concrete beams, as well as studying the effect of prestraining and the effect of SMA rebar diameter variability. They concluded that because smaller diameters provided a greater contact surface, it was preferable to use small diameterspresented a study of the performance of Ni-Ti SMA cables for use in reinforced concrete applications. Because of their excellent super-elastic properties, the cables were determined to have limitless applications. Nonetheless, in terms of bonding tests, The cable behaved differently than the conventional rebars or cables for which these tests were designed. The cable's low modulus of elasticity made it unsuitable for use in

reinforced concrete members. However, the modulus of elasticity can be increased by adjusting the alloy or heat treatment process to reduce transformation temperatures, thereby avoiding excessive longitudinal and transverse deformations and improving bonding properties, (Mas et al., 2017).

The prestressing of beams with a standard Ni-Ti alloy and a Ni-Ti-Nb alloy was investigated. They concluded that, in the specific case of the used SMAs, the latter was able to maintain recovery stresses after cooling the SMA, making it much more appropriate for prestressing, (El-Tawil & Ortega-Rosales 2004).

In tensile reinforcement, SMA wires were combined with conventional steel, and temporary prestressing was performed with the SMA to facilitate permanent reinforcement through CFRP laminates. They discovered that SMA wires can effectively reduce residual strain in beams after heating, but that combining them with steel impeded recovery. Ordinary SMAs' low modulus of elasticity precludes their use in conjunction with conventional steel arranged in the same direction, because the recovery stresses would be resisted by the steel with small deformations and would not be transmitted to the concrete. (El-Tawil and Ortega-Rosales, 2004)

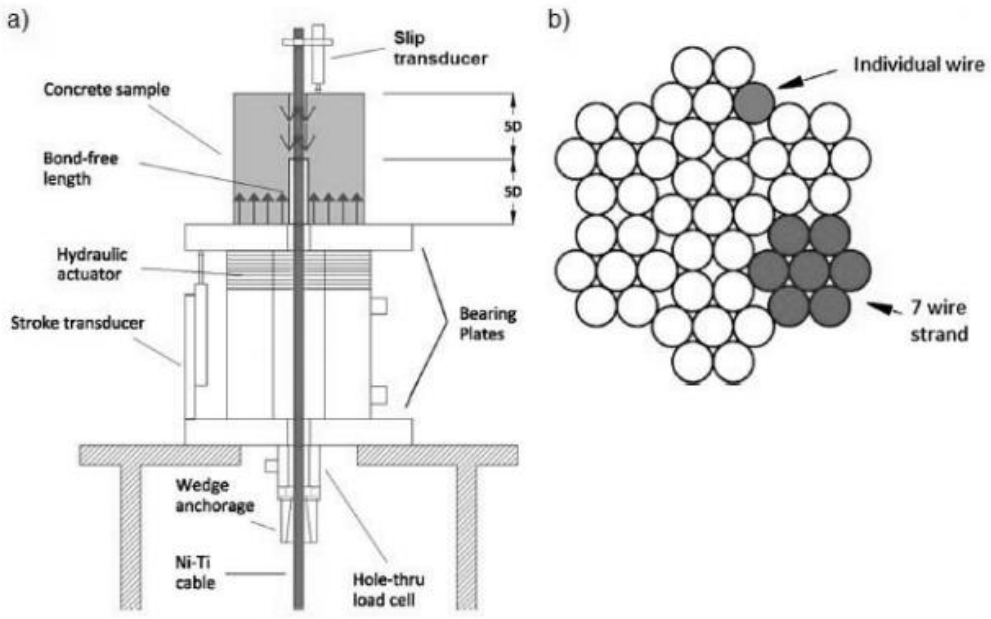

Figure 3: The use of SMAs as external prestressing for strengthening structures allows for the use of most SMAs' exceptional corrosion resistance characteristics.

Furthermore, because the alloy is applied to the concrete from the outside, it can reach high Af temperatures without causing damage to the concrete. There are, however, fewer research studies in this field. It is worth noting the reinforcement of a bridge in Michigan using SMA rebars via external post-tensioning.(Soroushian et al., 2001)following after a laboratory research study on the possibilities of external reinforcement of shear cracks.

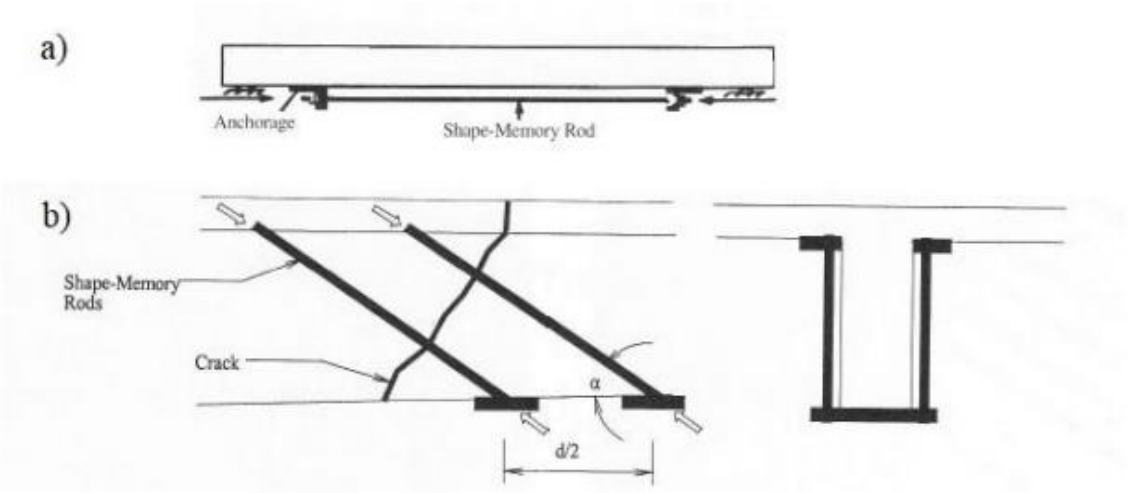

Figure 4: Figure Some analyzed possibilities of external reinforcement from(Soroushian et al., 2001): a) longitudinal corrective force and b) local post-tensioning for enhancement of shear resistance

Internal post-tensioning was used in a beam with self-rehabilitation capability, presenting the concept of reinforced concrete smart structure and its application in structural damage and rehabilitation, combining the use of SMAs and piezoceramic sensors for this. The structure was reinforced with Ni-Ti in martensite phase within post-tensioned sheaths, and tensioning up to 2% strain was applied. Cracking was detected by the piezometric elements. Once the damage was identified, the SMA cables were heated to 90 oC, causing the reverse transformation, adding tension to the SMA and thus compressing the concrete, (Song et al., 2006).

investigated the actual results of flexural behavior of RC beams reinforced and prestressed with Fe.SMA strips, comparing externally bonded reinforcement with near surface strengthening (strips located in grooves and filled with mortar to bond), taking advantage of reduced corrosion, fire, vandalism, mechanical damage, and aging.

The bond behavior was deemed adequate for strengthening purposes, with approximate recovery stresses of around 200 MPa, albeit lower than those obtained in the climate chamber of around 230 MPa under ideal conditions.(Shahverdi et al., 2016)

The Near Surface Mounted (NSM) technique (figure 2.23) had already been explored, and practical applications, such as in the case of FRP for RC structures, had been developed (De Lorenzis& Teng 2007).In addition, the NSM approach has been applied to Fe-based SMAs.

Also worked on flexural strengthening of RC beams using the NSM approach; with the advantage of isolating SMA bars/strips from the environment, they were put in a groove on the tension side of the RC beam (figure 2.23) and then activated by heating to apply prestressing force to the beam via the Fe-SMA The cracking load increased by 20.3%, 24.3%, and 18.3%, respectively.

yielding load and ultimate load, and 19.2% in yielding deflection from the reinforced beam to the weakening one They also noted that the Fe-SMA remained in good contact.

Using the grout until debonding at about yielding load(Rojob and El-Hacha, 2017.)

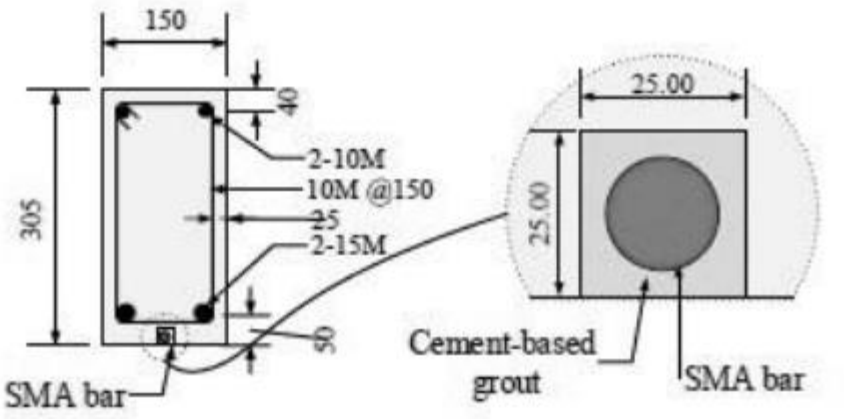

Figure 5: Section and detail of NSM SMA bar for prestressing technique. From(Rojob and El-Hacha, n.d.)

2.4.2 Active Confinement

Active confinement makes sense in the rehabilitation of existing buildings where ductility is required, but the expense of SMAs would hardly justify their use in the planing of new structures.(Janke, 2005)

In 2008, The behavior of concrete test specimens confined by 1 mm diameter wires was investigated. They employed two Ni-Ti alloys: one in martensite phase with a prestrain of 3%, which actively compressed the test specimens when heated through an electrical circuit, and another in austenite phase. The active confinement of the first example enhanced the concrete compressive strength marginally while increasing the ductility significantly. The austenite alloy created a similar confinement effect. It is worth mentioning that the geometrical flaws of the wire resulted in considerable losses once the martensite was cooled, which likely reduced the confining stress. (Choi et al., 2008)
dkjthk(Shin and Andrawes, 2012)

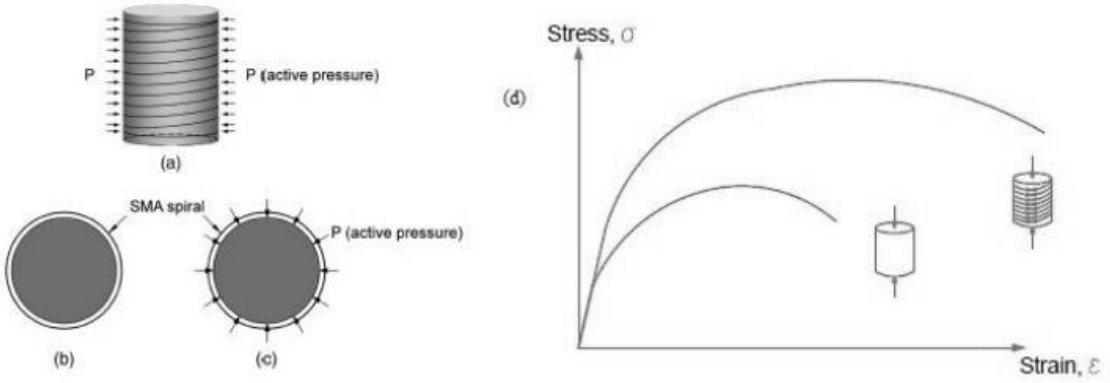

Figure 6: Schematic drawings of a confined concrete column uniaxial compressive test: a) Concrete element confined with SMA spirals, b) Cross-section before heating, c) Cross-section after heating, and d)Uniaxial compressive test stress–strain path comparison between confined and unconfined test. From(Cladera et al., 2014) , adapted from (Shin and Andrawes, 2010)

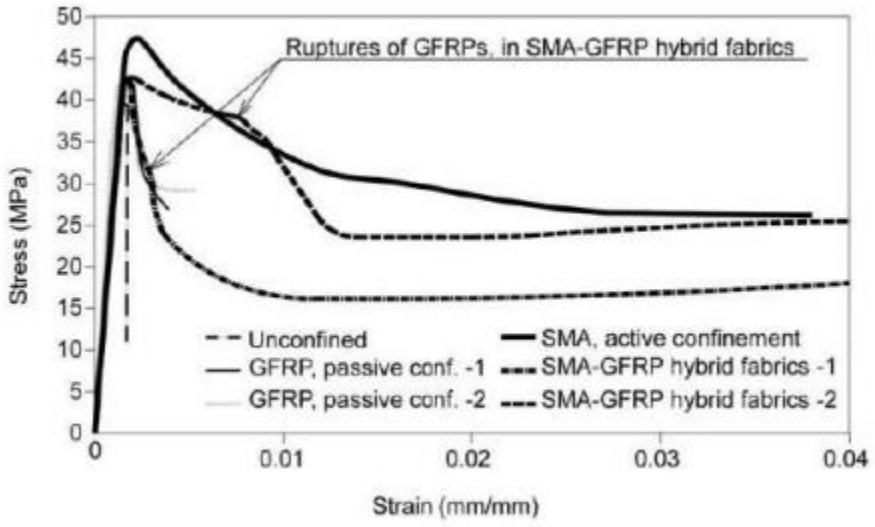

Figure 7: The stress-strain relationship for test specimens without confinement, as well as those confined using SMAs, GFRP, or SMA-GFRP hybrid fabrics.

In 2012 Found a maximum recovery stress of 574 MPa for Ni-Ti-Nb wires with an acceptable level of stability from -10 to 50 degrees Celsius (Dommer and Andrawes, 2012). Other SMAs may be useful for this purpose as well, as reported Fe-based SMA recovery stresses of around 500 MPa, (Leinenbach et al., 2012).

Ni-Ti-Nb wires have been successfully employed to actively confine circular and non-circular columns in order to enhance their behavior under axial compression stresses and bending.(Shin and Andrawes, 2010 ;(Dommer and Andrawes, 2012) reported good performance in retrofitting, i.e. seismic retrofit of highway bridge columns, on active confinement of RC columns (compression) using Ni-Ti-Nb spirals (following figure (a)).. A study of the application of Ni-TiNb martensitic SMA wires to retrofit reinforced concrete columns with lap splices using wire jackets yielded satisfactory results (following figure (b)). They also compared the results to those of Ni-Ti wires used in the same application. Furthermore, the study looked at the recovery and residual stresses of Ni-Ti-Nb wires, as well as their behavior. The study found that Ni-Ti-Nb wire jackets were more adaptable for RC column retrofit than Ni-Ti wire jackets because Ni-TiNb had better acceptable temperature windows for SMA applications in civil constructions. (Choi et al., 2012)

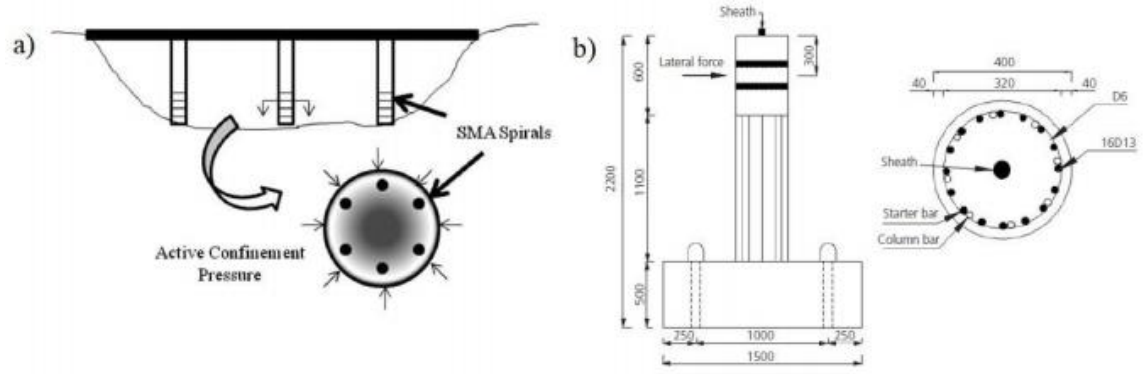

Figure 8: Ni-Ti-Nb wires, (Choi et al., 2012)

2.4.3 Performance of recovery stresses

One critical issue is the development of recovery stress under non-ideal constraints during the installation or activation of SMA components. The development of predicted recovery stresses in the presence of an initial gap, or contact defect.

elastic restraints or between the concrete surface and wires (non-circular RC components) diminished, and the reinforcement's efficacy may be affected or directly disabled if The strain was initially lost when it reached a specific value.

The generation of recovery stresses in a constrained Fe-based SMA utilized for mechanical coupling was investigated. On the other side, prestressing was studied with a focus on non-ideal restrictions that might decrease stress recovery. The development of recovery stresses in the presence of an initial gap and elastic restrictions was explored experimentally (figure 2.29). The results indicated that even under non-ideal restraining circumstances, the alloy could still produce significant recovery stresses, and that the ultimate recovery stress decreases almost linearly with decreasing strain.(Lee et al., 2015).

2.4.4 Active strengthening of RC beams using Ni-Ti-Nb

If a SMA is employed as external reinforcement, such as to wrap a beam, and the recovery strain is restricted while heating and cooling, the SMA will create recovery stresses, prestressing and/or constraining the concrete member. These pressures will be

imposed throughout the structure's service life if the SMA is properly selected.(Gibert, 2019)

Because of its pseudo-elastic behavior and damping capacity, Ni-Ti alloys have previously been employed in a variety of civil engineering applications. However, as previously discussed in this chapter, the alloy's short thermal hysteresis makes it unsuitable for use in prestressing applications in civil engineering constructions that rely on the shape memory effect. (Mas et al., 2016).

The usage of Ni-Ti-Nb wires as shear critical beam prestraining reinforcement may overcome the limitation of a narrow hysteresis.

Chapter 3: Modeling

3.1 Overview

Numerical investigation of structures offers an attractive technique ofresearch due to low cost, quick results and ability to study several variables in depth. As a result, using the commercial software ABAQUS, a three-dimensional non-linear F.E. a simply supported beam model is created.

The material parameters for this model will be provided in the verification and parametric study chapters, while this chapter presents a general description of an R.C simply supported beam modeling.

The modeling of the joint involves material specification, creation of parts, modeling of interfaces, selection of analysis regime, loading setup, boundary conditions and meshes as explained in the following subsections.

3.2 Material modeling

In this section, constitutive models for concrete and steel under compression and tension loads are presented. Also, a constitutive model for SMA bars is included.

3.2.1 Concrete

Concrete is a non-homogeneous material that is difficult to simulate due to the variation in material response at various stages of loading in both tension and compression. The effect of crushing and cracking on concrete strength and stiffness can be approximated in a variety of ways. One method is to incorporate these effects into the stress-strain behavior of concrete using the "Concrete Damaged Plasticity" model (CDP).

The CDP model, which is included in the ABAQUS software, is used to simulate the complex nonlinear behavior of concrete. This model takes into account two major failure criteria: tensile cracking and compressive crushing of the concrete material as in following figure.

The CDP captures strength and stiffness degradation in concrete via tension and compression damage parameters (dt,dc), as shown in figure bellow. (ABAQUS User Manual, 2013).

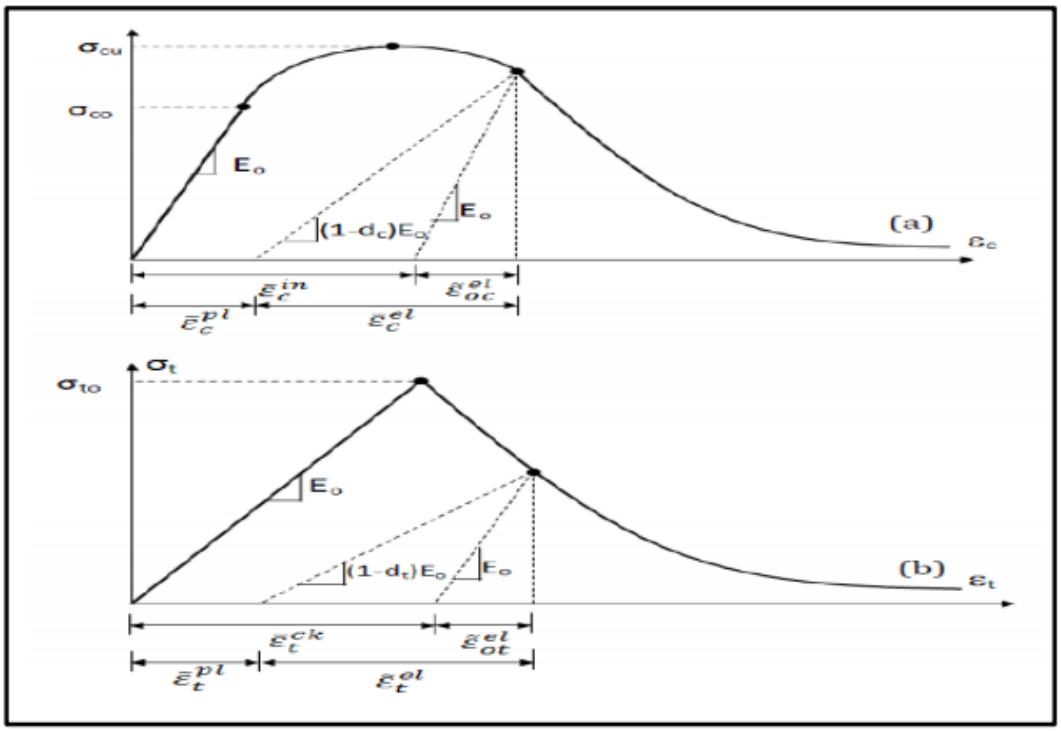

Figure 9: Response of concrete to uniaxial loading in (a) compression and (b) tension (Simulia, 2013)

The unloaded response of a concrete specimen is weakened, as shown above, because the elastic stiffness of the material is damaged or degraded due to cracks. Two damage variables, dt and dc, with values ranging from zero to one, characterize the degradation of elastic stiffness on the strain softening branch of the stress-strain curve. One denotes total loss of strength, while zero represents undamaged material. E0 is the material's initial (undamaged) elastic stiffness, and $\varepsilon c\sim pl$, $\varepsilon t\sim pl$, $\varepsilon c\sim in$, $\varepsilon t\sim in$ are compressive plastic strain, tensile plastic strain, compressive inelastic strain, and tensile inelastic strain, respectively. The elastic relations under uniaxial tension (σt) and compression (σc) are considered in Equations (3.1) and (3.2). (3.3)

$$\sigma t = (1-dt).E0.(\varepsilon t - \varepsilon t\sim pl) \quad (3.1)$$

$$\sigma c = (1-dc).E0.(\varepsilon c - \varepsilon c\sim pl) \quad (3.2)$$

The effective tensile and compressive cohesion stresses are utilized to calculate the yield point using the yield function. The yield function proposed by Lubliner et al. (1989) is used in the model, with revisions proposed by (Lee and Fenves, 1998).to account for

different evolution of strength under tension and compression under multi-axial loading case.

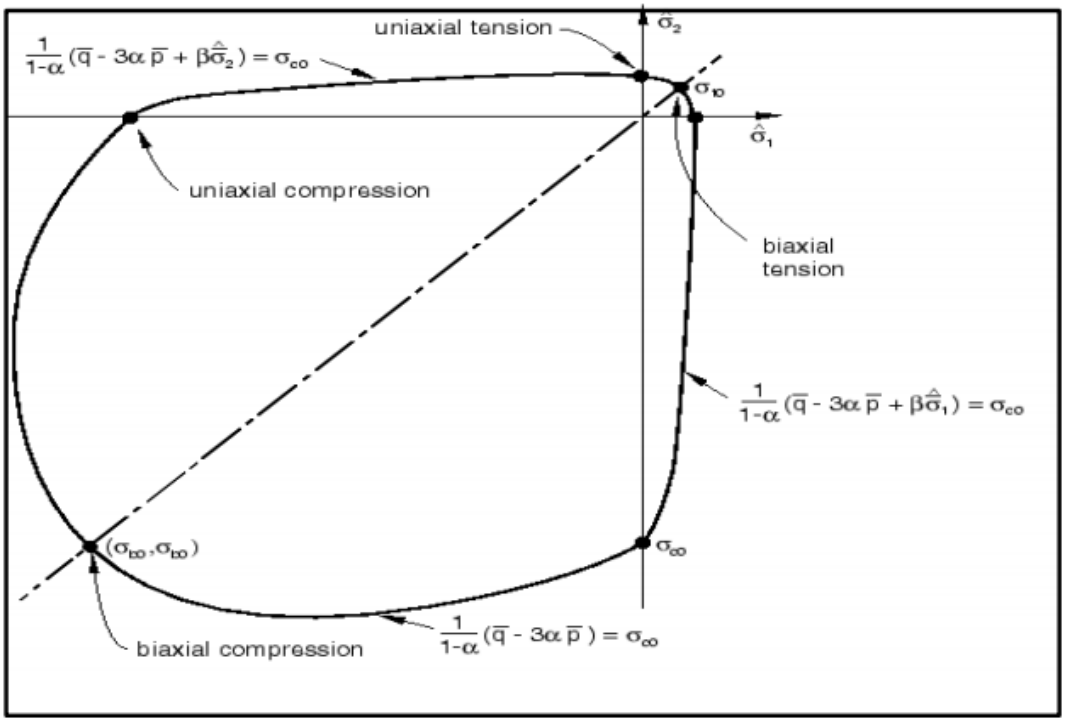

Figure 10: Yield surface in plane stress (Simulia, 2013)

As a result, the material model incorporates the confinement effect caused by tri-axial stress data in concrete, allowing for an increase in compressive capacity in the case of a hydrostatic stress condition.

Uniaxial Compression Behavior: Many researchers proposed equations that describe the behavior of concrete under uniaxial compression stress in general. Most of these equations, including those proposed by Mander et al., 1988 and Yong et al., 1988, do not explain the entire stress-strain curve of concrete. As a result, as shown in Equation, the stress-strain equation established by Saenz, 1964 and confirmed by Asran et al., 2016 is utilized to define the entire behavior of concrete under uniaxial compressive stress (3.3).

33

$$\sigma_c = \frac{E_c \varepsilon_c}{1+(R+R_E-2)\frac{\varepsilon_c}{\varepsilon_0}-(2R-1)\left(\frac{\varepsilon_c}{\varepsilon_0}\right)^2+R\left(\frac{\varepsilon_c}{\varepsilon_0}\right)^3} \quad (3.3)$$

$$E_c = 4700\sqrt{f`_c} \quad (3.4)$$

$$R = \frac{R_E(R_\sigma-1)}{(R_\varepsilon-1)^2} - \frac{1}{R_\varepsilon} \quad (3.5)$$

$$R_E = \frac{E_c}{E_0} \quad (3.6)$$

$$R_\sigma = \frac{f`_c}{\sigma_f} \quad (3.7)$$

$$R_\varepsilon = \frac{\varepsilon_f}{\varepsilon_0} \quad (3.8)$$

$$E_0 = \frac{f`_c}{\varepsilon_0} \quad (3.9)$$

Where:

σ_c: Concrete compressive stress (MPa)

E_c: Modulus of elasticity of concrete (MPa)

E_0 : Secant modulus of concrete (MPa)

$f`_c$: Maximum compressive strength of concrete (MPa)

ε_c: Compression strain

ε_0: Strain corresponding to $f`c$ which is equal approximately 0.0025 asreported by Hu (1989).

ε_f: Maximum strain.

σ_f: Stress at maximum strain (MPa).

R : Ratio relation

R_E : Modular ratio.

R_σ: Stress ratio, which is equal 4 as reported by Hu (1989).

R_ε: Strain ratio, which is equal 4 as reported by Hu (1989).

Tension behavior: Sharif et al., 2016 experimentally test the stress-strain curve for concrete under tension for concrete 25MPa. According to ACI 318, the maximum tensile

stress was reported as 2.9MPa, corresponding to the modulus of rupture of concrete, which is equal to $0.62\sqrt{f`c}$. With this load, the flexural capacity of concrete began to drop until the final strain reached 0.003. Asran et al., 2016 used this equation in ABAQUS to define the tension behavior of concrete, assuming linear decreasing tension. This model takes into account a maximum tensile strain of 0.003 under flexural test for all types of concrete.This assumption is used due to lack of sufficient information about ultimate strain in tension of concrete from experimental tests which will be used for verification purpose.

According to CDP, modeling concrete requires many parameters in order to capture the behavior of concrete accurately. These parameters are summarized below:

1- Poisson's Ratio (ν) : the amount of transversal elongation divided bythe amount of axial elongation. A value of 0.2 is used in the model.

2-Young's Modulus (Ec): Modulus of elasticity of concrete (MPa).

Equation (3.4).

3- Dilation angle (internal friction angle). In other words, it is the anglemeasured in the p–q plane (hydrostatic pressure stress – Misesequivalent effective stress) at high confining pressure as shown in figure below (Simulia, 2013). In simulations usually ψ= 36° or 40° is recommended by Kmiecik and Kamiński, 2011.

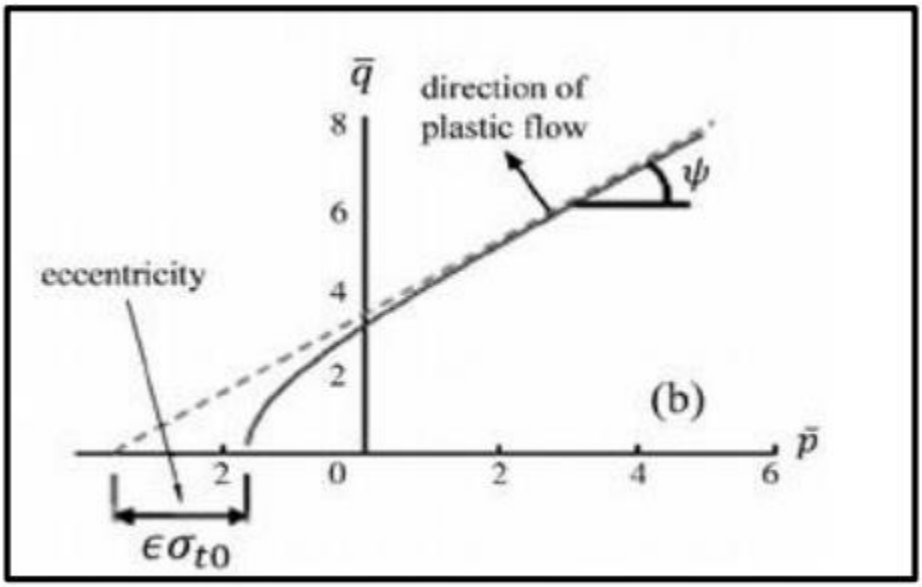

Figure 11: Dilatation angle and eccentricity Simulia, 2013

4- Eccentricity: parameter that defines the rate at which the flowpotential function approaches the asymptote in p-q plane. The CDPmodel recommends assuming this value equal 0.1 Simulia, 2013. When this value equals 0 then the surface in the meridian plan becomes straight line similar to the classic DruckerPrager hypothesis as shown in Figure above, (Simulia, 2013).

5- $fb0/fc0$: bi-axial compression stress divided by uni-axial compressionstress. Kupfer (1969) conducted experimental test and obtained that thisratio is equal to 1.16.

6- K: represents the ratio of the distances between the hydrostatic axis and both the compression and the tension meridians in the deviatoric cross section which is equal 2/3 which is recommended by (Simulia, 2013). This factor is used to convert the shape of cross

section of failure surface from circle to combination of three mutuallytangent ellipses as shown in the following figure (Simulia, 2013) . This shape was formulated by (Willam and Warnke, 1975).

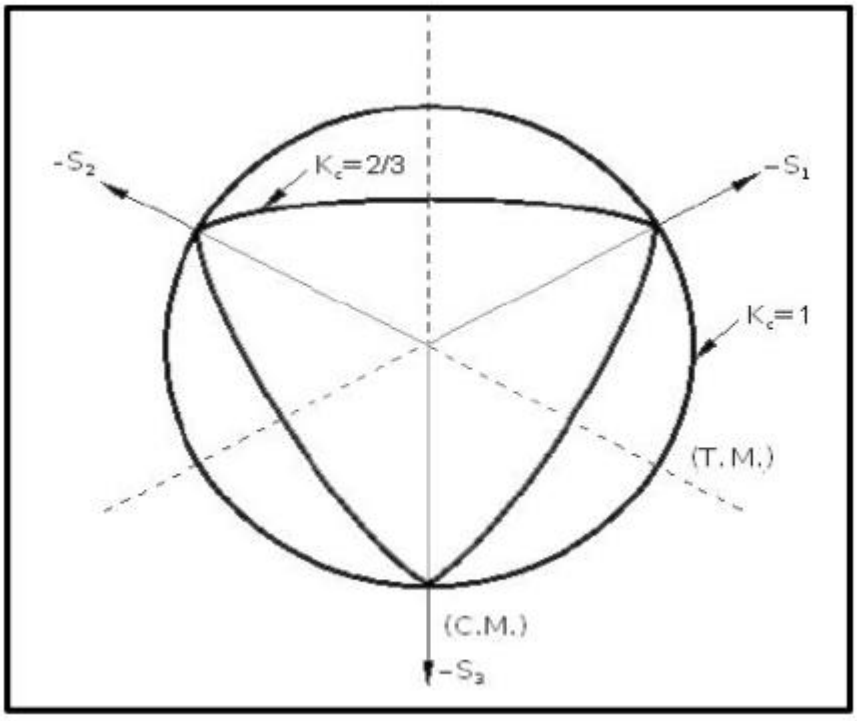

Figure 12: Deviatoric cross section of failure surface (Simulia, 2013)

7- Compression stress versus inelastic strain curve: Compression yieldstress versus inelastic strain curve used in this thesis as an input datafor definition CDP model.

8- Tension yield stress versus cracking strain curve: Tension yield stressversus Cracking strain curve used in this thesis is thesis as an inputdata for definition CDP model.

9- Compression damage parameter (dc): This parameter represents thedegradation of the elastic stiffness due to compression in concrete.dc is defined as the ratio between the inelastic strain (crushing strain)and total strain (Wahalathantri et al., 2011).

10- Tension damage parameter (dt): This parameter represents thedegradation of the elastic stiffness due to tension in concrete. dt isdefined as the ratio between the cracking strain and total strain (Wahalathantri et al., 2011).

11- Tension recovery (ωt) and compression recovery (ωc): These arematerial properties that control the recovery of the tensile and compressive stiffness upon load reversal. The experimentalobservation in most quasi-brittle materials, including concrete, is thatthe compressive stiffness is recovered upon crack closure as the loadchanges from tension to compression. On the other hand, the tensilestiffness is not recovered as the load changes from compression totension once crushing micro-cracks have developed. This behavior, which corresponds to ωt =0 and ωc = 1, is the default used byABAQUS. Uniaxial load cycle (tension-compression-tension) withdefault values for the stiffness recovery factors: to ωt =0 and ωc = 1as shown in following figure (Simulia, 2013).

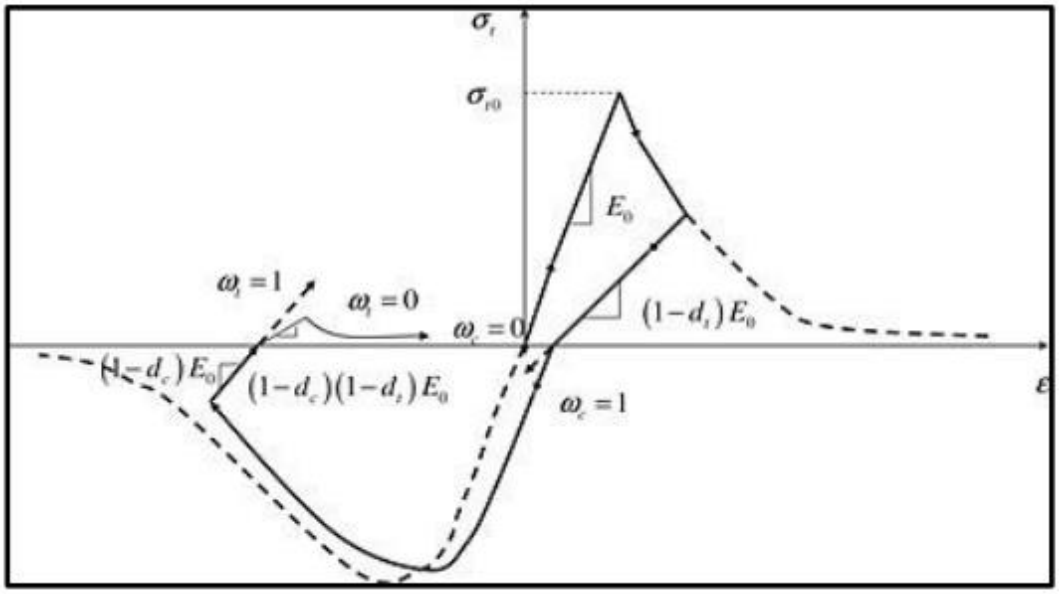

Figure 13: Uniaxial load cycle (tension-compression-tension) assuming default values for the stiffness recovery factors: to ωt =0 and ωc = 1 (Simulia, 2013)

3.2.2 Steel

Generally, steel is initially linear-elastic for stress less than the initial yield stress. At ultimate tensile strain, the reinforcement begins to neck and strength is reduced. At a maximum strain, the steel reinforcement fractures and load capacity is lost.

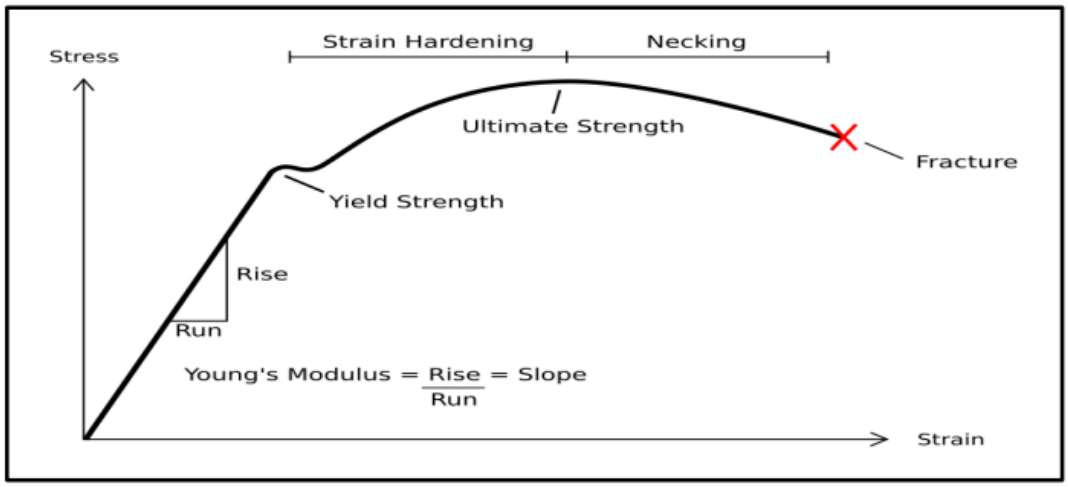

Figure 14: Typical stress-strain curve of steel

An isotropic behavior was used to model the reinforcement and loadingplate. This mean that the yield surface changes size uniformly in alldirections such that the yield stress increases (or decreases) in all stressdirections as plastic straining occurs.

3.2.3 Shape memory alloys (SMA):

Metallic alloys that have the ability to recover their original shape after undergoing large deformations, when the temperature is increased specific level.If a SMA is employed as external reinforcement, such as to wrap a beam, and the recovery strain is restricted while heating and cooling, the SMA will create recovery stresses, prestressing and/or constraining the concrete member. These pressures will be imposed throughout the structure's service life if the SMA is properly selected.

3.3 Analysis type, loading and boundary conditions

In ABAQUS, pseudo-dynamic analysis is used to acquire the full behavior and avoid the convergence problem. As a result, in order to reach the static solution, load is applied in very large time steps. Employing dynamic analysis rather than static analysis aids in the convergence of highly nonlinear cohesive contact behavior in ABAQUS.

Figure below shows a schematic view of the model's boundary conditions and load. The beam load is applied through displacement control at rate of 2 mm/s at the tip of beam.

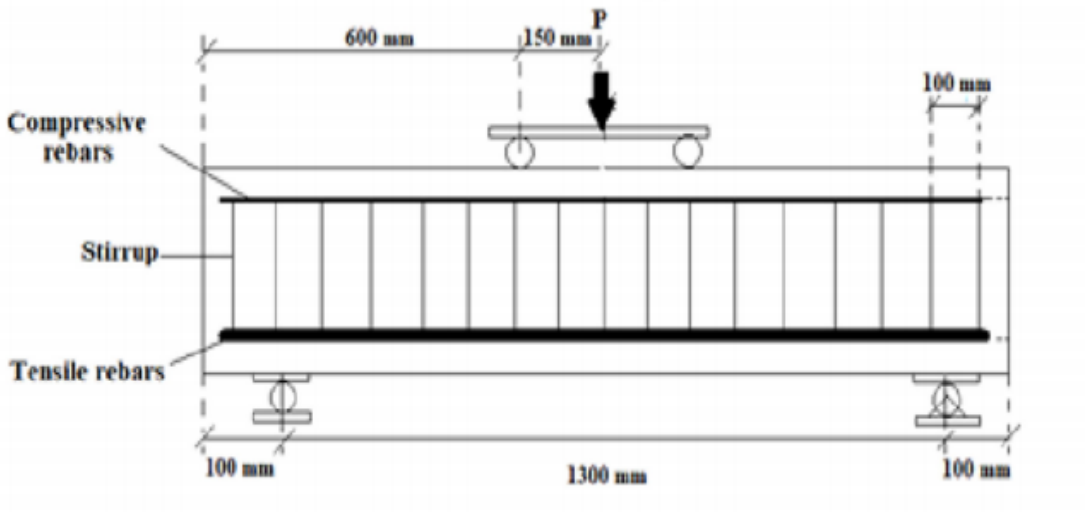

Figure 15: Location of loads and boundary conditions

3.4 Meshing types

The components of beam are meshed individually on part-by-part basis instead of using global or sweep mesh. Eight- nodded linear brick element (C3D8R) is used to model the solid elements; concrete and loading plate. A 2-node linear 3-D truss element is used to model main and transfers reinforcement (T3D2), whereas 4-noded shell element (S4R) used to model SMA as shown in figure:

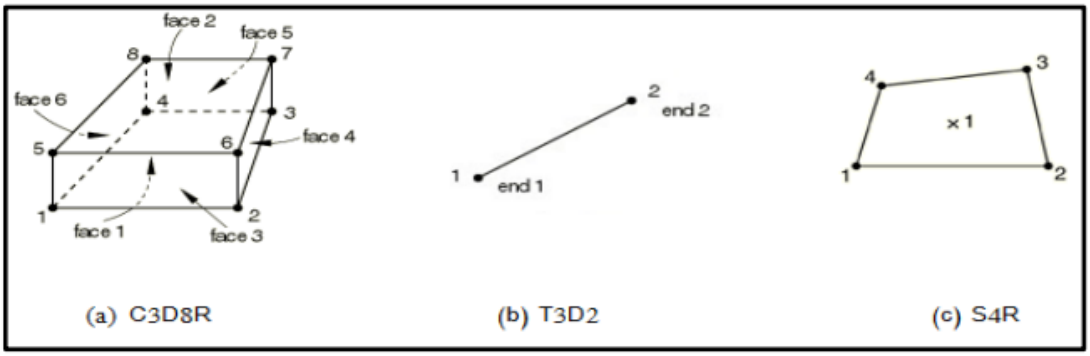

Figure 16: Finite Element Meshing Types

Chapter 4: Experimental Program

4.1 General

Data from experimental tests are used to validate the finite element model results. However, there are various experiments on R.C beams. Many of these experiments have not been reported in detail and are therefore difficult to model. A well-documented set of experiments is chosen to validate the results of the FE model. Many independent tests reported in the literature are used to determine the validation. One of them is an R.C beam subjected under four – point static load (displacement control) which was tested by (Karimipour and Edalati, 2020).

4.2 Beam geometry and reinforcement

According to the selected paper, the Reinforced Concrete beam has a cross-section that is 150 mm wide, 200 mm high, and a length of 1500 mm. This beam is reinforced with two phi10 compression bars on top, two phi20 tension bars on the bottom, and with phi8/100mm stirrups in the beam we intended to strengthen against flexure. There are no stirrups in the beam, which we intended to strengthen against shear.

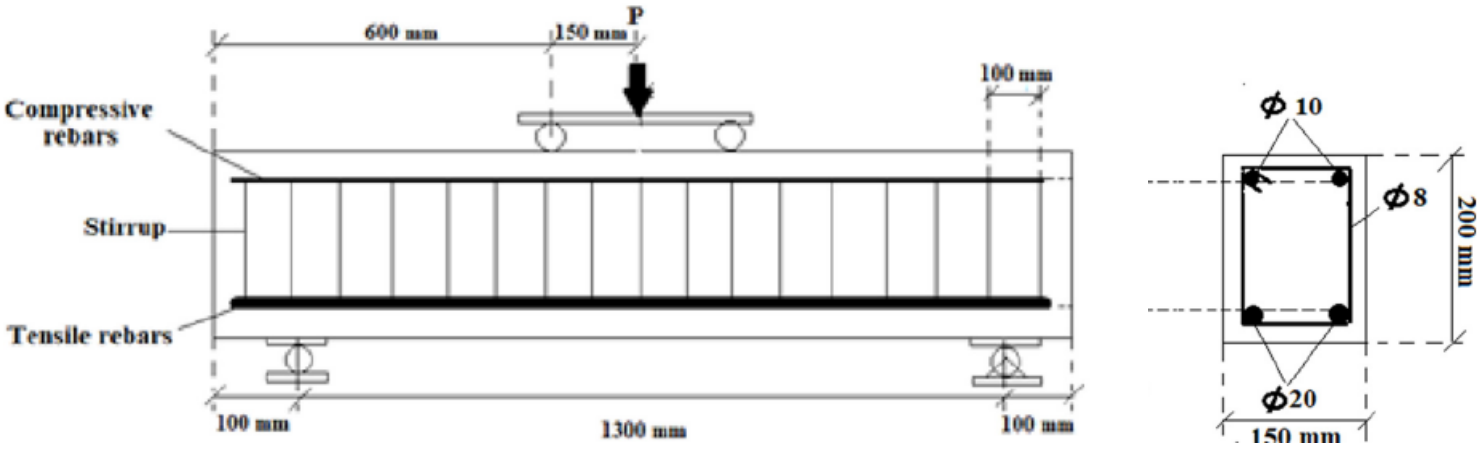

Figure17: Studied Beam

4.3 Specifications of materials used

Reinforcement and dimensions details for tests done by (Karimipour and Edalati, 2020)are illustrated in Chapter 2 in this thesis. Steel bars have a modulus of elasticity of 200,000 MPa and a Poisson's Ration of 0.3. For the SMAs, the modulus of elasticity and Poisson's Ratio were set to 105,000 MPa and 0.2 respectively. The paper provides the following information about the properties of rebars used:

Table 2: Rebar Properties

Rebar diameter	**Yield strength**	**Ultimate strength**	**Yield strain**	**Ultimate strain**	**Modulus of elasticity**
mm	**MPa**	**MPa**	**%**	**%**	**GPa**
8	371	545	0.1294	24.93	209.28
10	371	571	0.1304	24.82	210.10
20	558	694	0.1527	25.51	213.17

The concrete compressive strength was determined by performing a compressive test during the experiment and was determined to be 36 MPa. Because The curves were not provided so Elkady's tool(Elkady, 2023)will be used in order to obtain data based on the Chinese Code (GB 50010-2010) as follows:

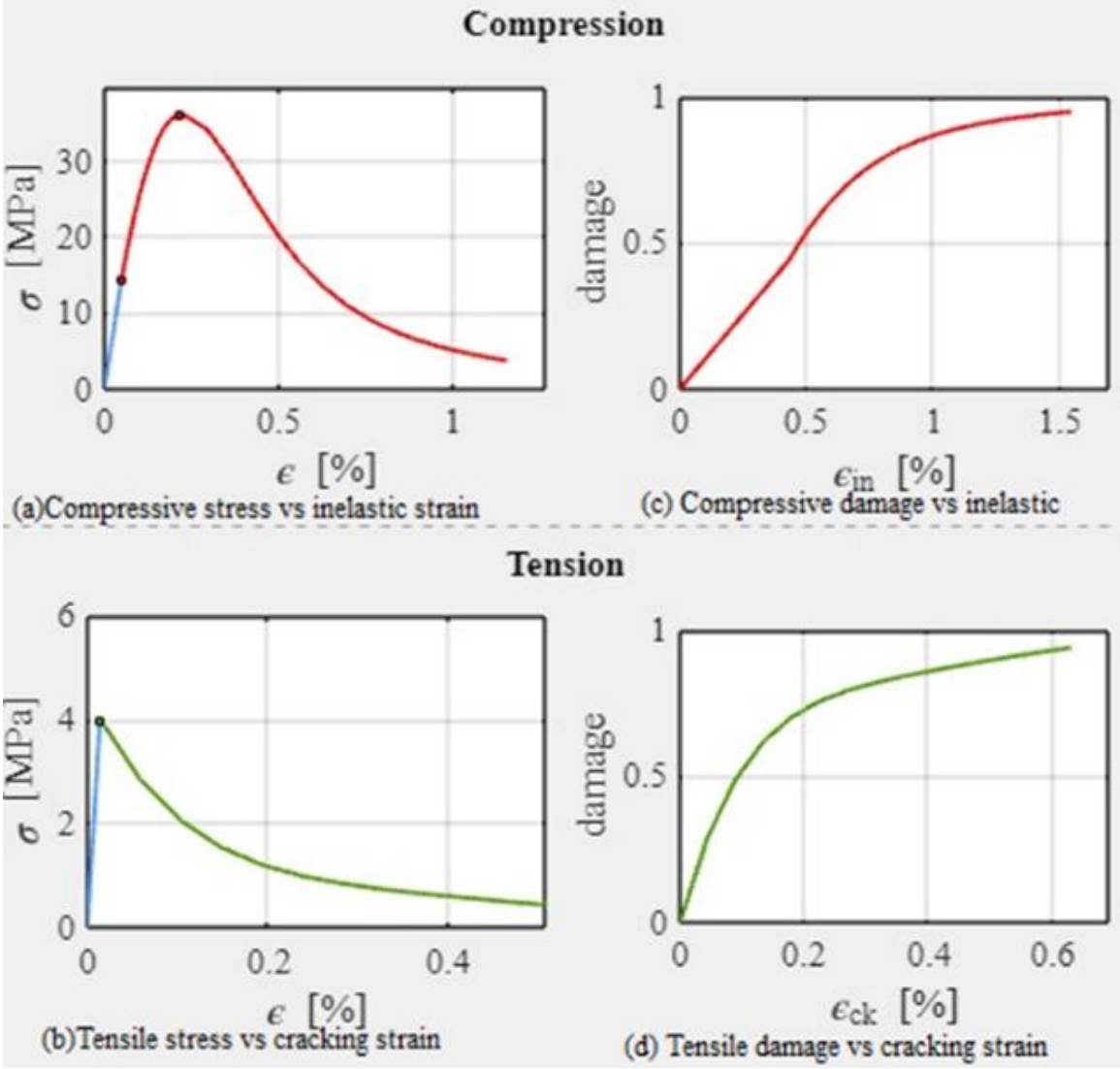

Figure 18: Elkady's Tool Data for 36 MPa Concrete

Table 4.2: Parameters of concrete used in test of Karimipour and Edalati (2020)

E_0(MPa)	ν	ψ	e	f_{b0}/f_{c0}	K
29139	0.2	36°	0.1	1.16	0.67

Table above shows the major parameters used in ABAQUS to define the behavior of a concrete model. However, last figure shows uniaxial compression stress-inelastic strain curve of concrete, tension stress-cracking strain curve of concrete with, compression damage parameter versus inelastic strain curve, and tension damage parameter versus cracking strain curve.

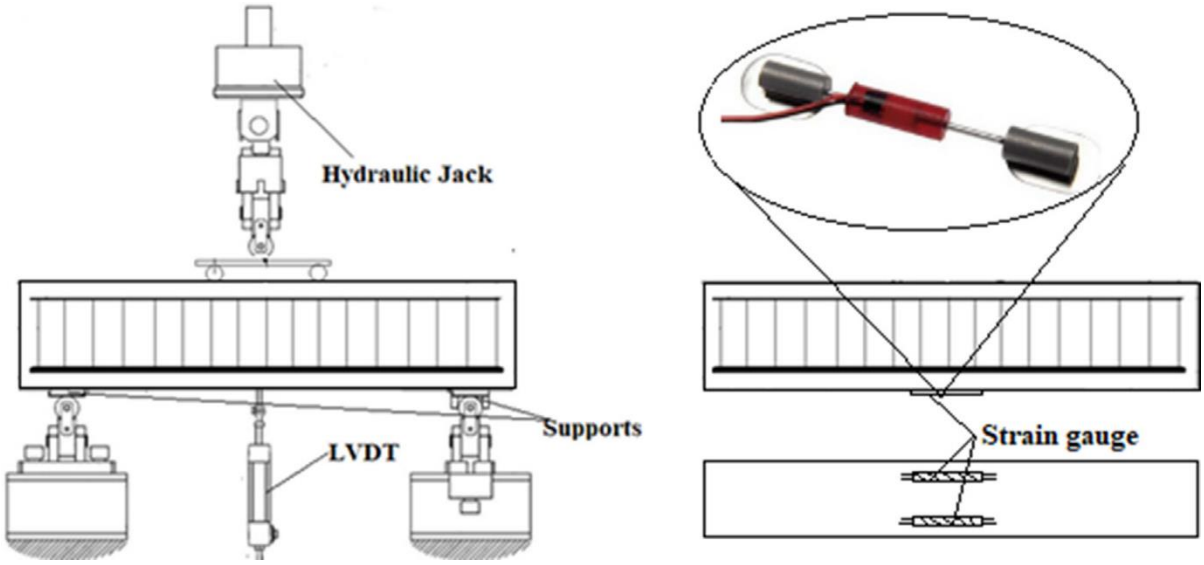

Figure 19: Experimental test setup, (Karimipour and Edalati, 2020)

4.4 Building and verification of model data

Abaqus was used by creating parts with the predefined dimensions and added materials' definitions, then by assigning each part creating and the corresponding material to new sections. To apply the load on and support the beam, a new part called "Steel Plate" has been added. To ensure that this component has no effect on the results, the modulus of elasticity defined as 10 times the normal steel's modulus (2,000,000 MPa) with relatively small dimensions. Then the parts assembled together to complete with the model shaped as the experiment. There were two load points separated by 300 mm, each with two supports, a roller and a pin.

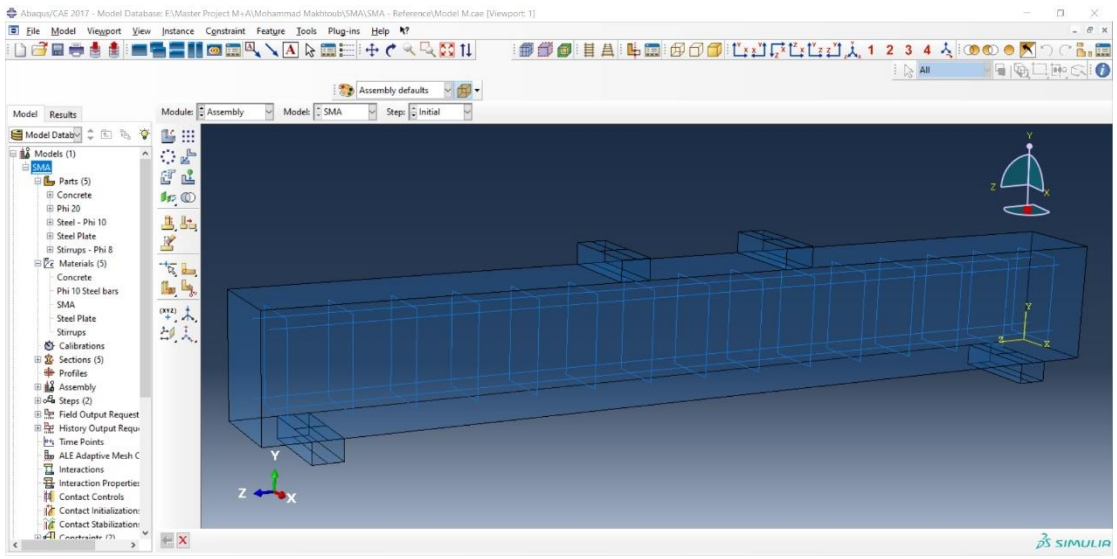

Picture 1: Parts menu and showing Reinforced Concrete Beam

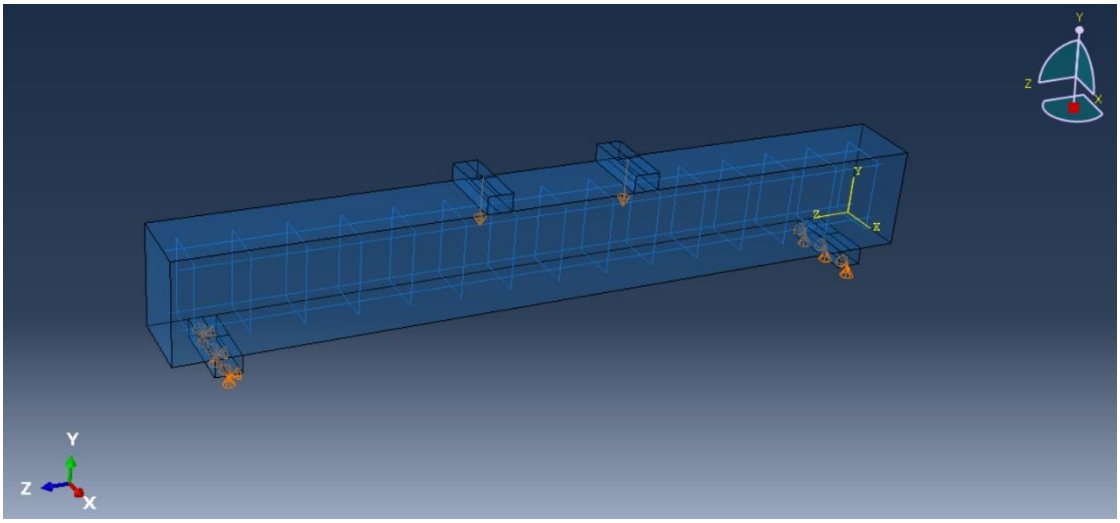

Picture 2: Original Model Load and supports' locations

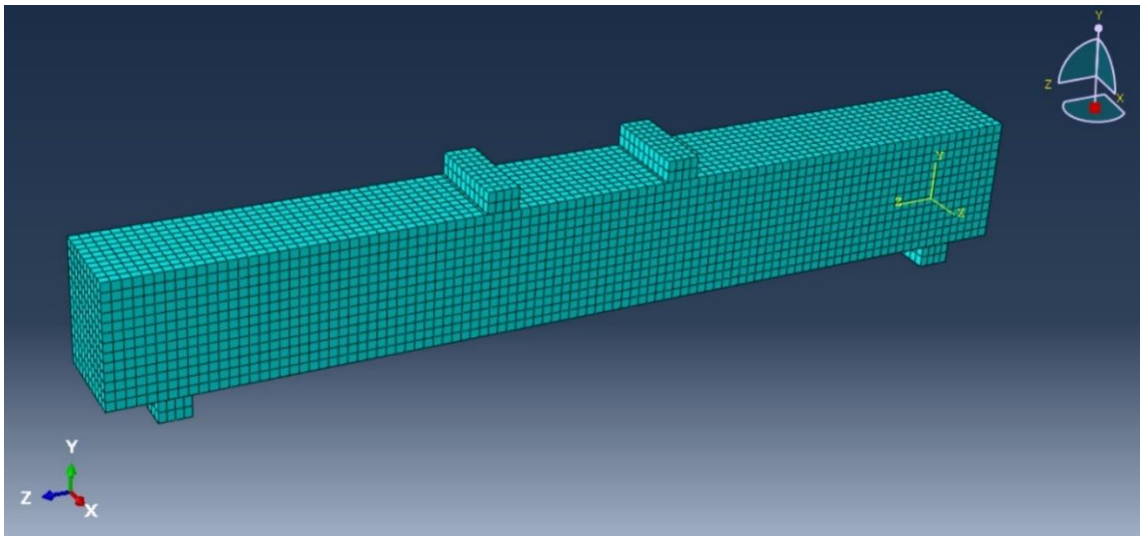

Picture 3: Meshing the whole model

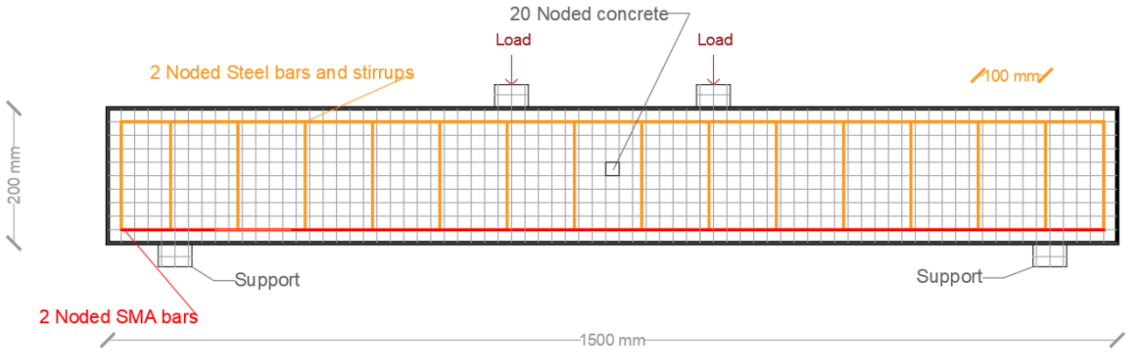

Figure 20: Meshing standards

To exclude the effect of mesh size on the results A sensitivity study performed. The materials specifications are expected to be the same as those specified (Karimipour and Edalati, 2020).Different general mesh sizes were considered (10 mm through45mm). The results show that the generated curves stabilize approximately mesh sizes 15-35 mm, as shown in following figure. However, a mesh size of 15 mm is used in all subsequent models to prevent divergence error in ABAQUS, which occurs in many models of 35/25 mesh sizes.

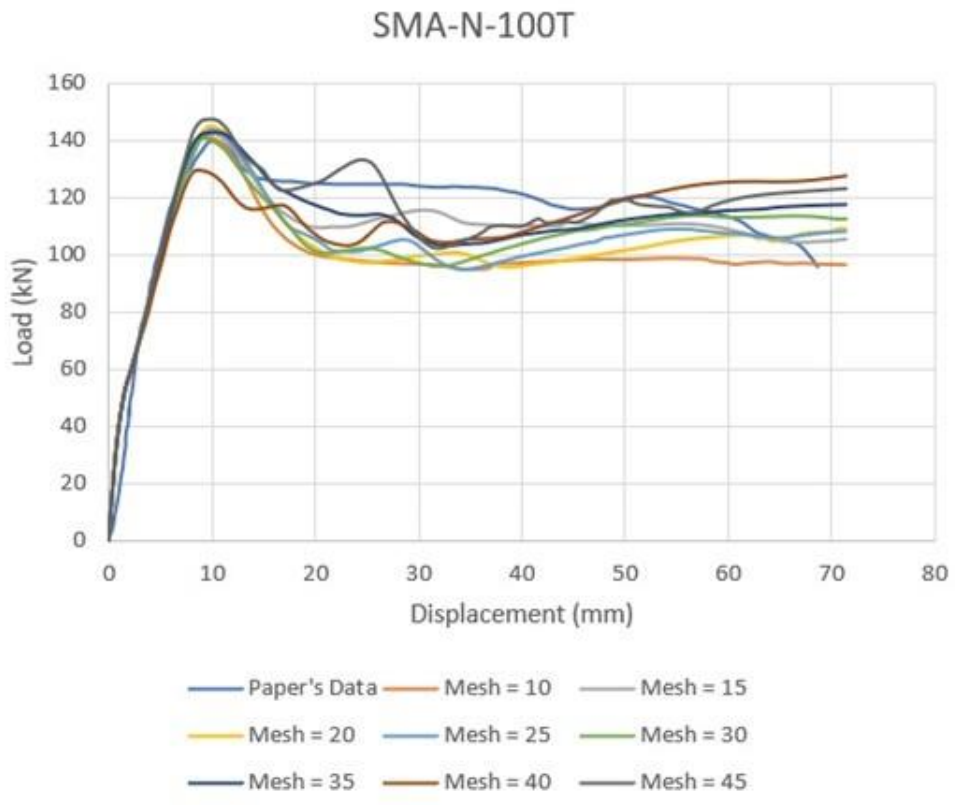

Figure 21: Load - Displacement Curve for different mesh sizes

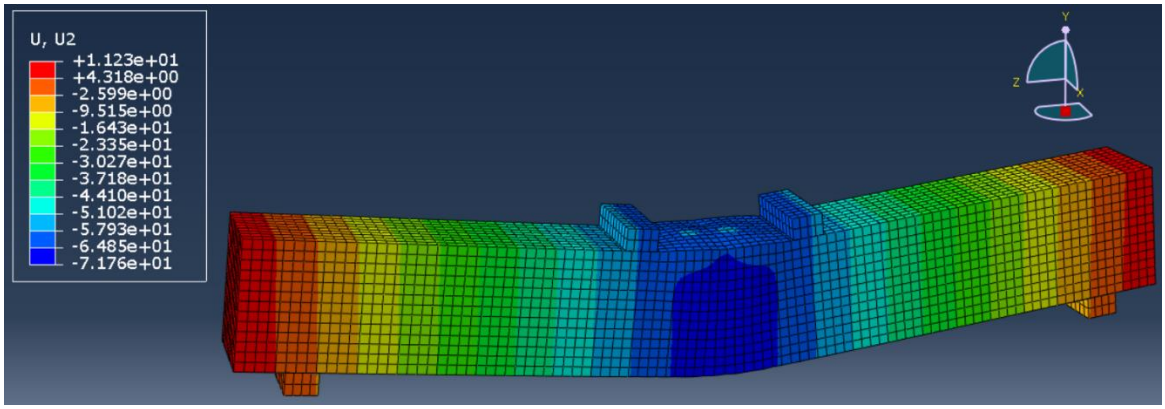

Picture 4: With SMA - U2 (Vertical Displacement)

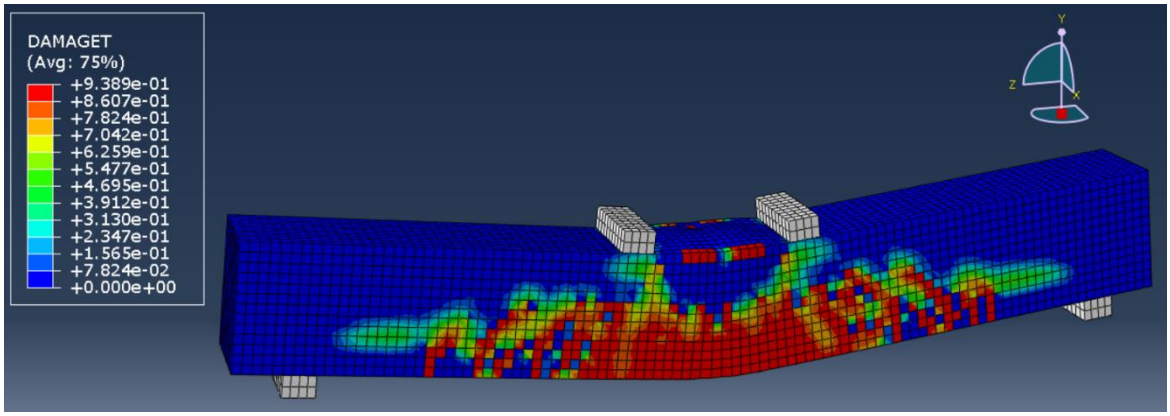

Picture 5: With SMA- Damage Tension

Picture 6: Experimental sample damage

As shown in the two above pictures, the damage in the concrete due tension is taking the same methodology. The cracks start from the bottom middle of the beam and moved on to the upper surface.

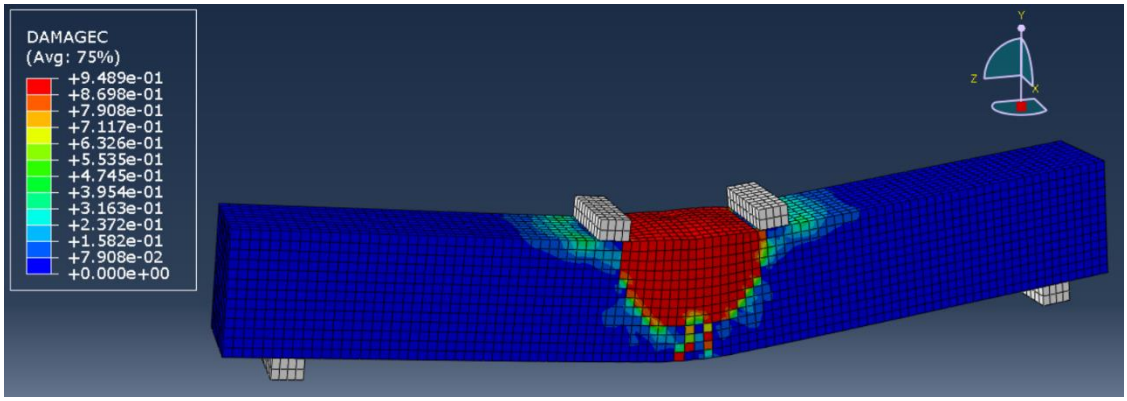

Picture 7: With SMA – Compression Damage

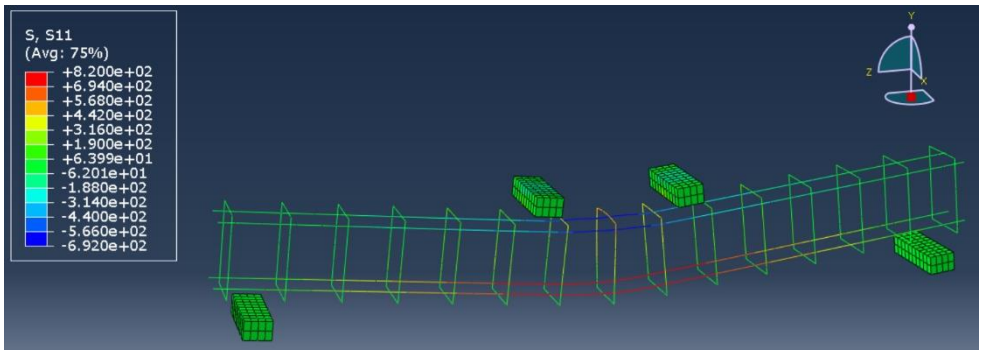

Picture 8: With SMA– Steel and SMA Normal Stress

In order to validate the accuracy and reliability of the numerical model, the numerical load-deflection curve due to static loading is compared with the envelopes of the loading hysteresis loops from the experimental test conducted by (Karimipour and Edalati, 2020). Comparison between F.E. and experimental results are shown in the next figure. It can be seen that the F.E. model captures the overall behavior quitesatisfactorily.

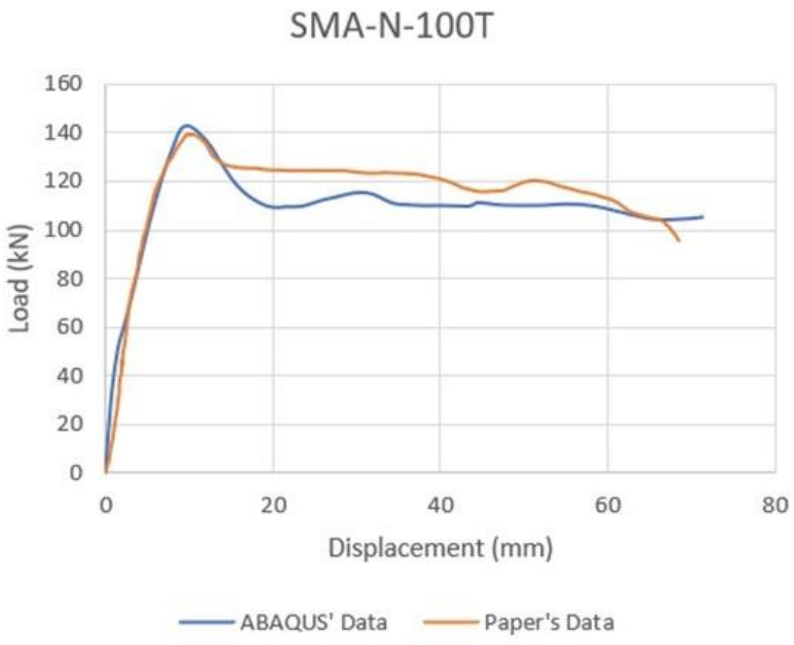

Figure 22: Load - Displacement Curve for original model

4.5 Parametric study

Parametric study is conducted to investigate the behavior of R.Cbeam strengthened by SMA. The behavior is affected by many parameters. These parameters are:

4.5.1 Changing the area of SMA bars

The SMA bars applied for resisting tension force were having different sizes as following:

4.5.1.1 Phi 16 SMA bars

Two phi 16 bars have the total area of 401.92 mm^2 will give us the following deflection:

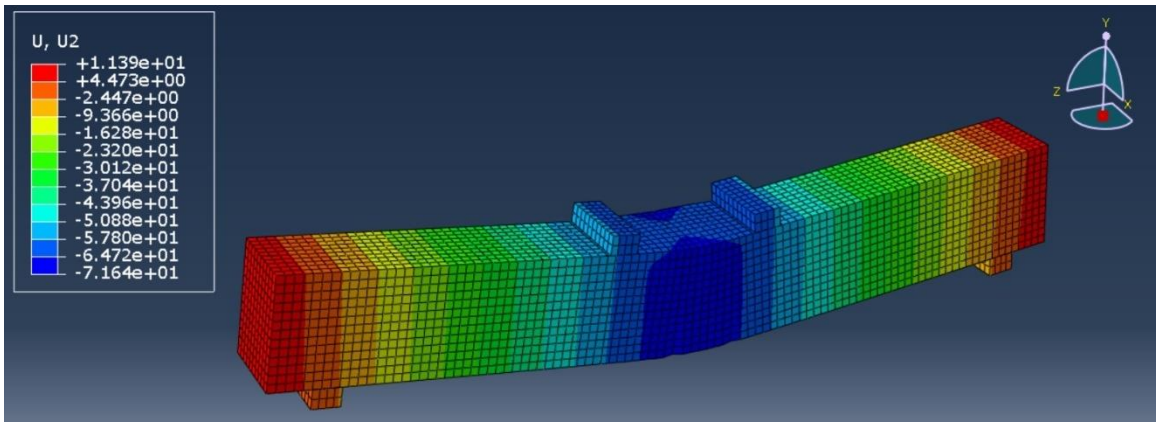

Picture 9: SMA-Phi16 Model - U2 (Vertical Displacement)

4.5.1.2 Phi 18 SMA bars

Two phi 18 bars have the total area of 508.68 mm^2 will give us the following deflection:

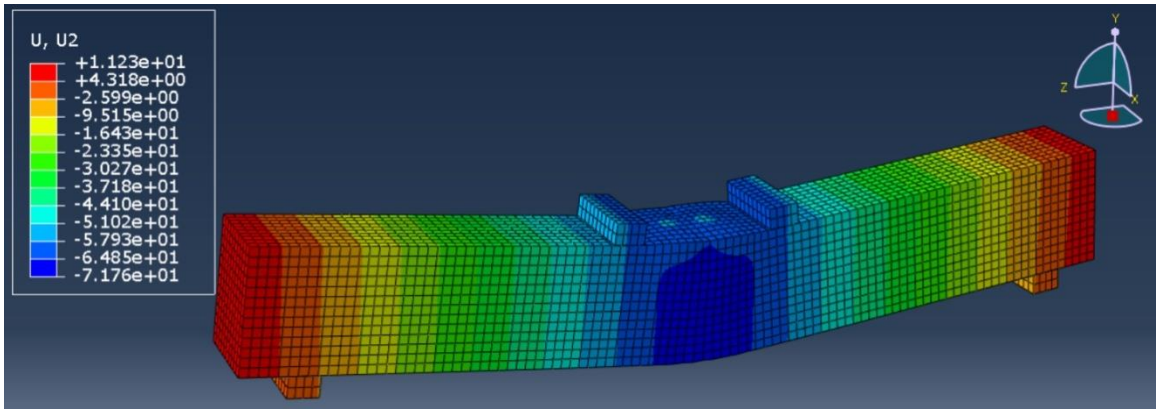

Picture 10: SMA-Phi18 Model - U2 (Vertical Displacement)

4.5.1.3 Phi 20SMA bars

This study is exactly the same of the original model.

4.5.1.4 Phi 22SMA bars

Two phi 22 bars have the total area of 759.88 mm^2 will give us the following deflection:

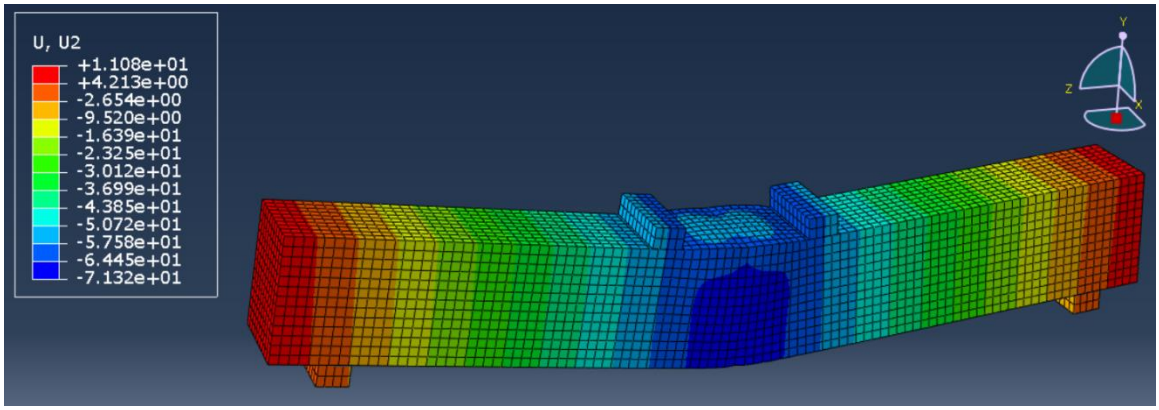

Picture 11: SMA-Phi22 Model - U2 (Vertical Displacement)

4.5.1.5 Phi 24SMA bars

Two phi 24 bars have the total area of 904.32 mm^2 will give us the following deflection:

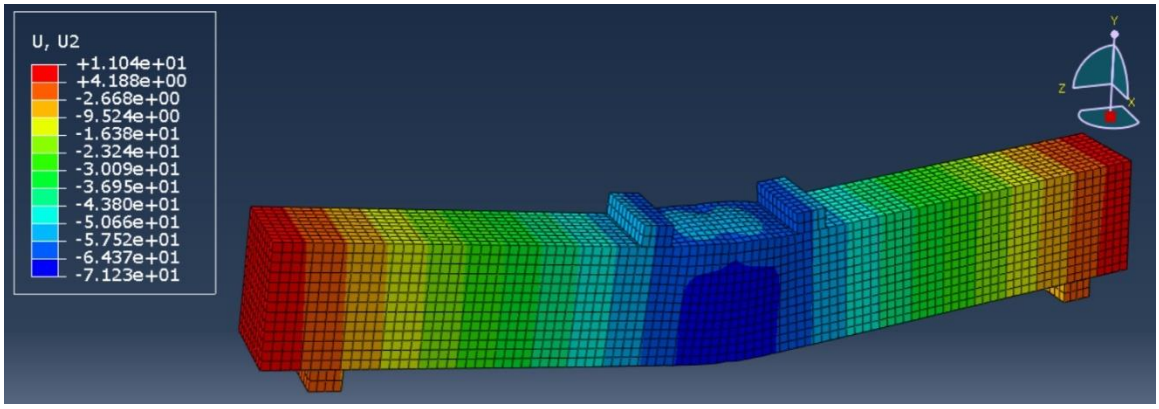

Picture 12: SMA-Phi24 Model - U2 (Vertical Displacement)

4.5.2 Changing distances between Loads

The load applied on the beam on two-upper points, the distance between these two points is changed. There are 5 models developed in this area:

4.5.2.1 Distance = 0 mm

Two phi 20 bars have the total area of 628 mm^2 will be used with no distance between the load points (only one point load in the middle of the beam) will give us the following data:

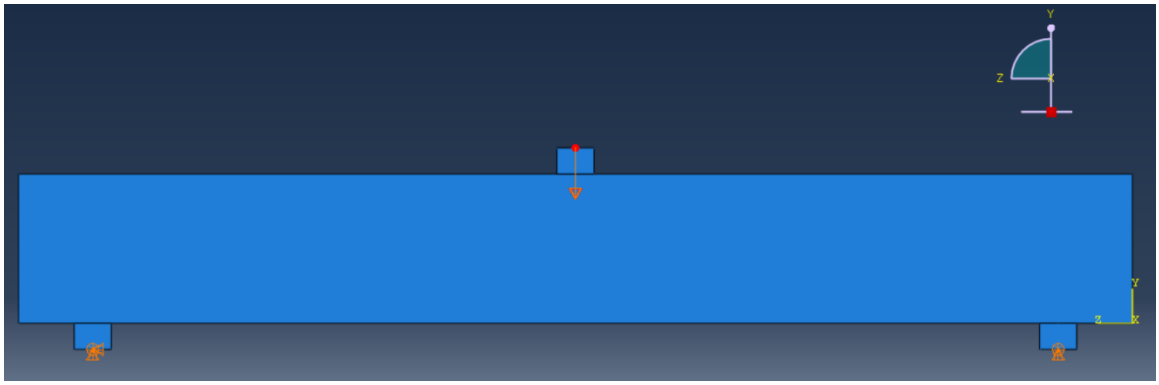

Picture 13: SMA-0 Model - Load and supports' locations

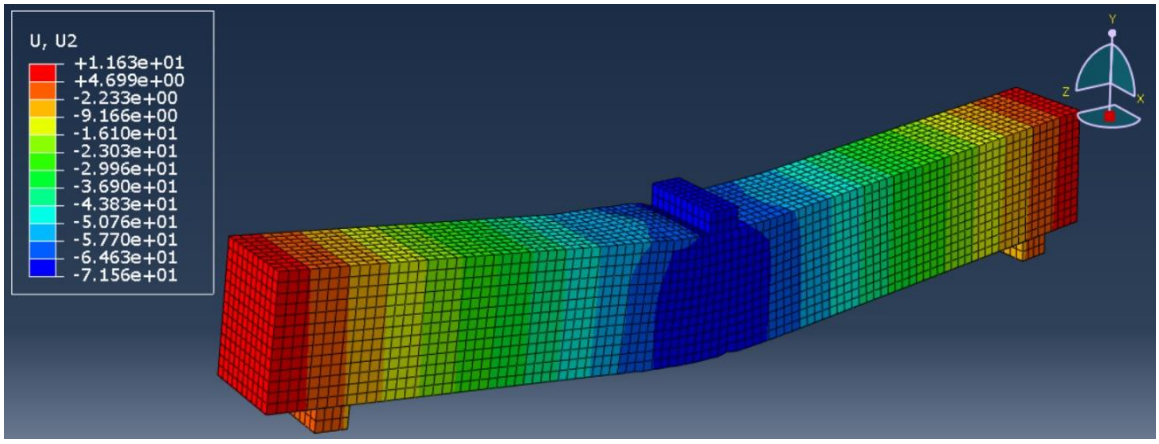

Picture 14: SMA-0 Model - U2 (Vertical Displacement)

4.5.2.2 Distance = 150 mm

Two phi 20 bars have the total area of 628 mm^2 will be used with distance between the load points equal to 150 mm will give us the following data:

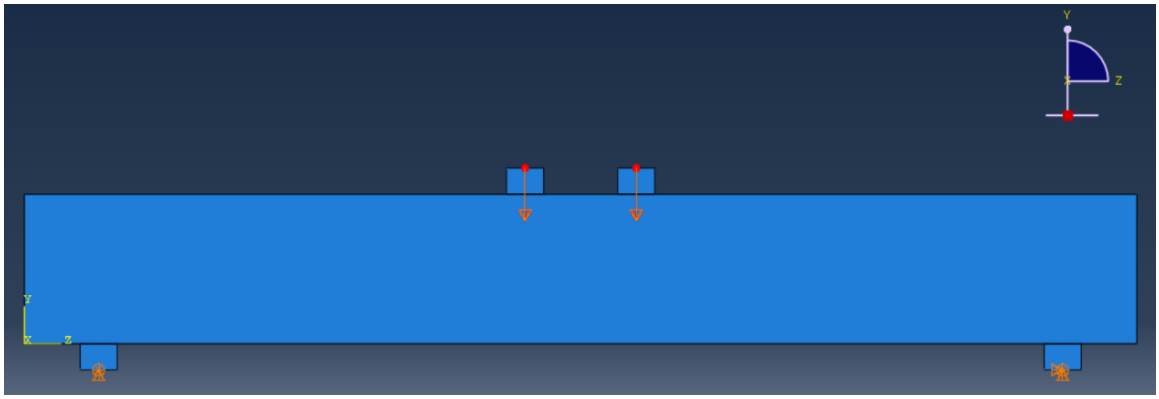

Picture 15: SMA-150 Model - Load and supports' locations

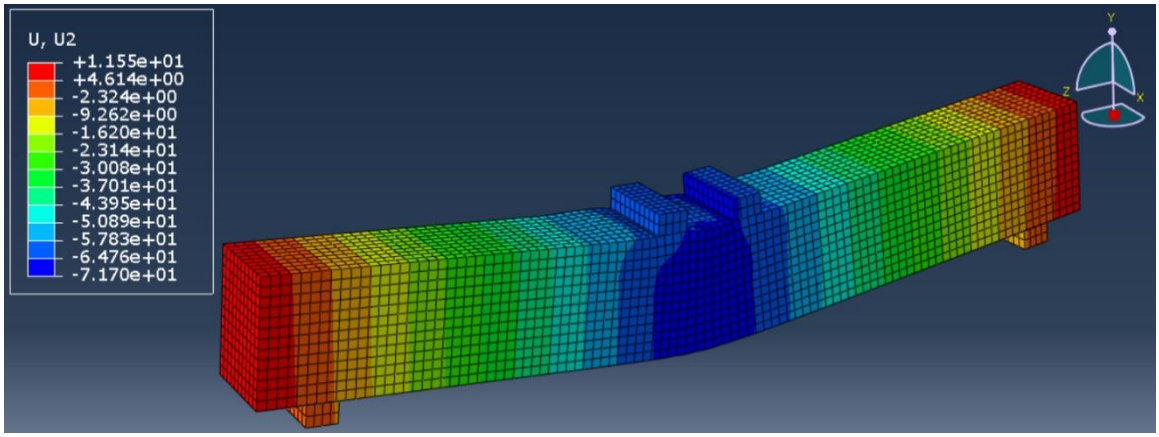

Picture 16: SMA-150 Model - U2 (Vertical Displacement)

4.5.2.3 Distance = 300 mm

This study is also exactly the same of the original model.

4.5.2.4 Distance = 450 mm

Two phi 20 bars have the total area of 628 mm^2 will be used with distance between the load points equal to 450 mm will give us the following data:

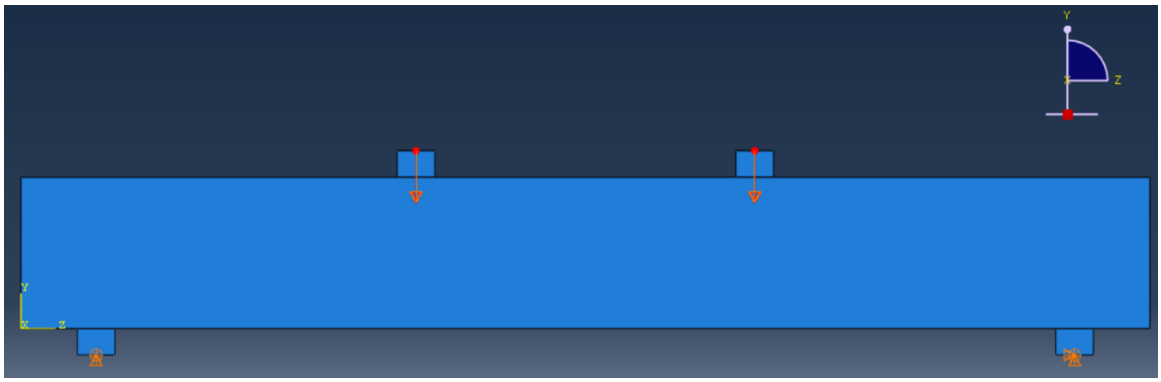

Picture 17: SMA-450 Model - Load and supports' locations

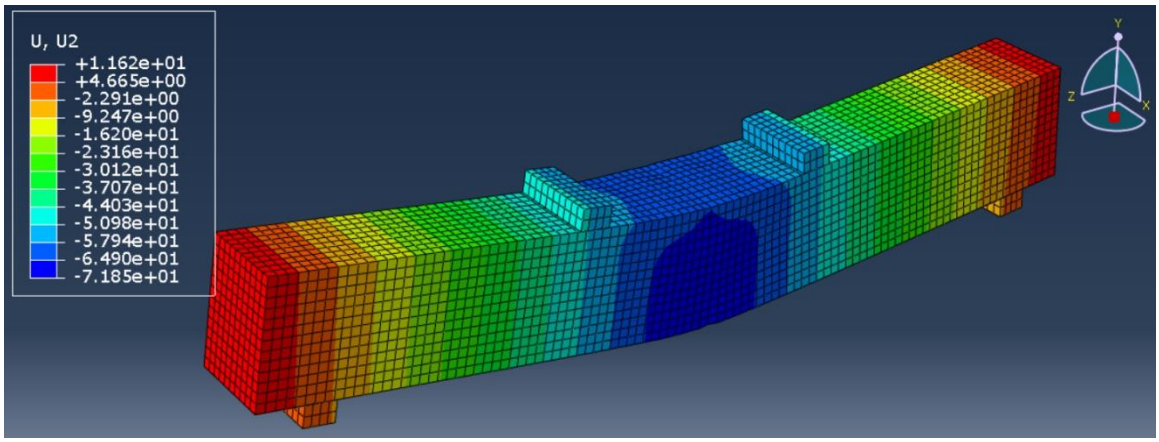

Picture 18: SMA-450 Model - U2 (Vertical Displacement)

4.5.2.5 Distance = 600 mm

Two phi 20 bars have the total area of 628 mm^2 will be used with distance between the load points equal to 600 mm will give us the following data:

Picture 19: SMA-600 Model - Load and supports' locations

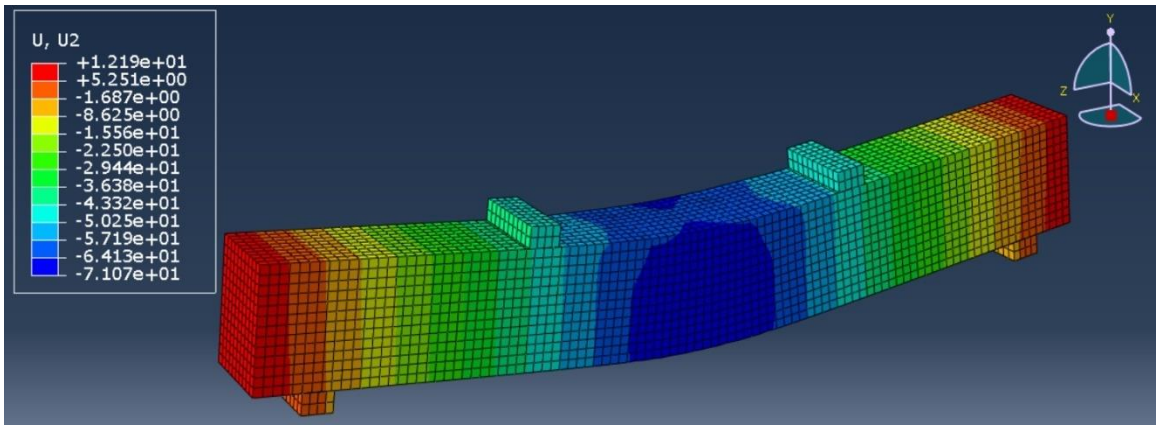

Picture 20: SMA-600 Model - U2 (Vertical Displacement)

4.5.3 Changing concretecompressive strength (f_c`)

The concrete strength was changed to examine the effect on the whole model strength as follows:

4.5.3.1 Concrete have the compressive strength of 20 MPa

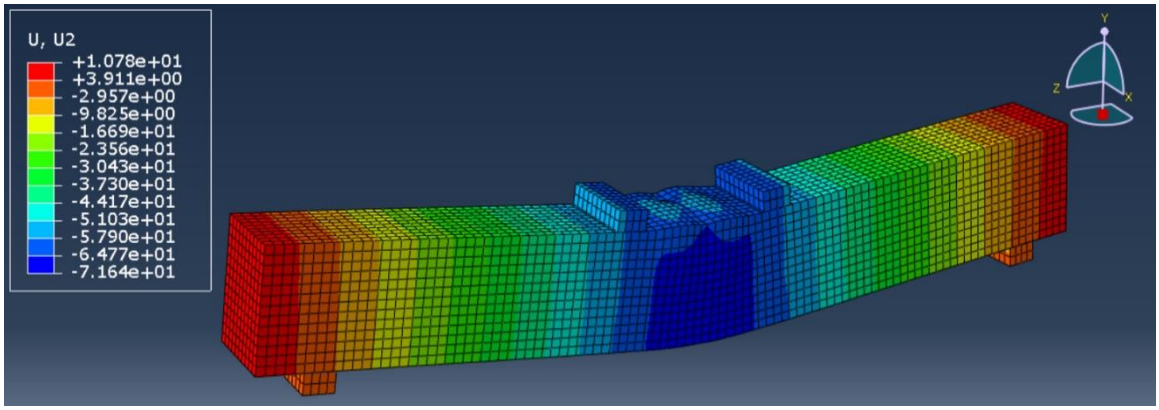

Picture 21: 20MPa-Concrete Model - U2 (Vertical Displacement)

4.5.3.2 Concrete have the compressive strength of 28 MPa

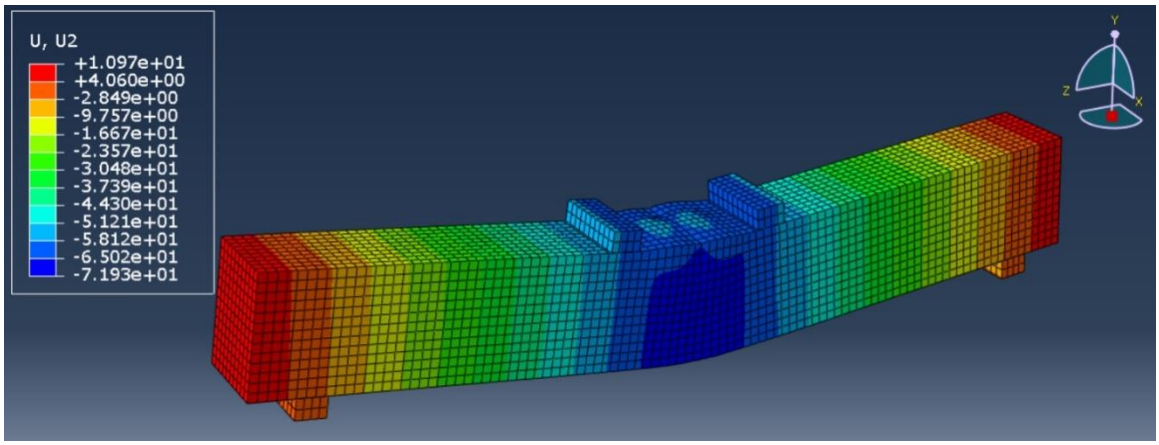

Picture 22: 28MPa-Concrete Model - U2 (Vertical Displacement)

4.5.3.3 Concrete have the compressive strength of 36 MPa

This study is also exactly the same of the original model.

4.5.3.4 Concrete have the compressive strength of 44 MPa

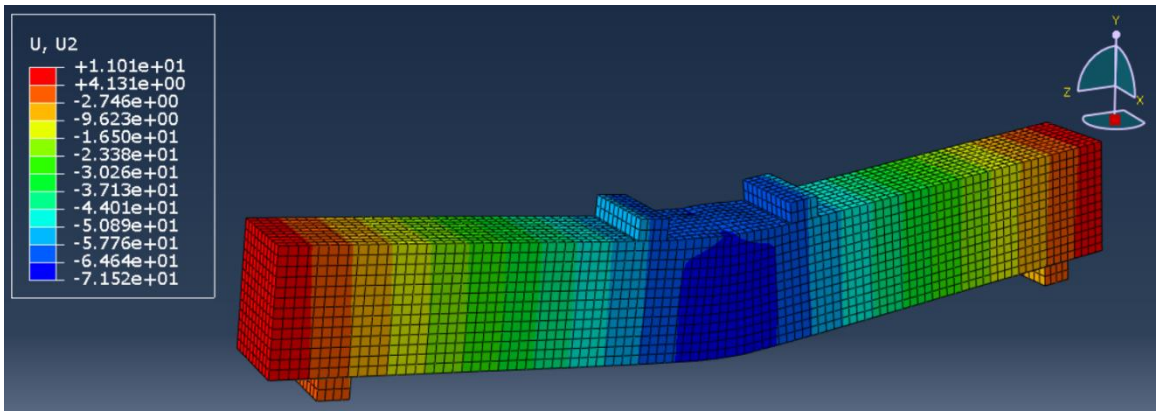

Picture 23: 44MPa-Concrete Model - U2 (Vertical Displacement)

4.5.3.5 Concrete have the compressive strength of 52 MPa

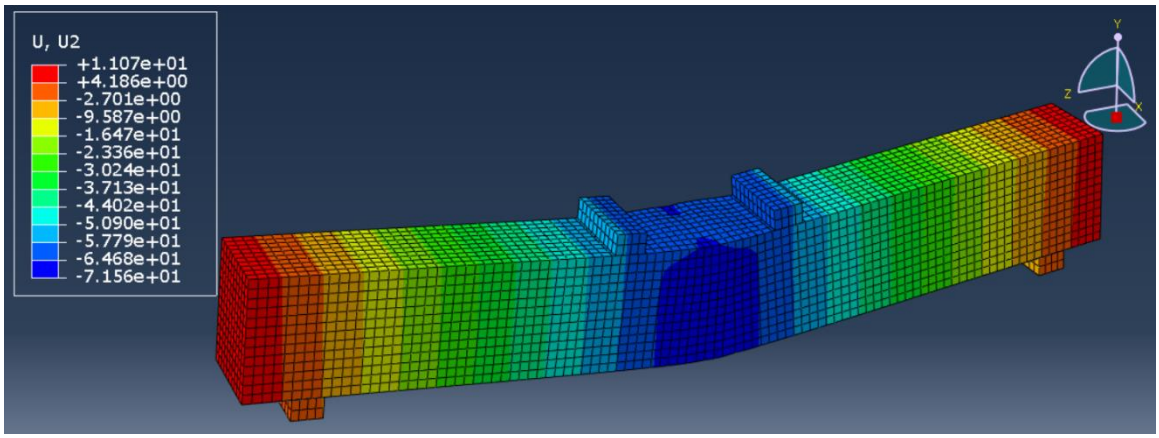

Picture 24: 52MPa-Concrete Model - U2 (Vertical Displacement)

Chapter 5: Results

5.1 Damage in tension

In this section, damaget (Tension Damage) will be shown for all models studied.

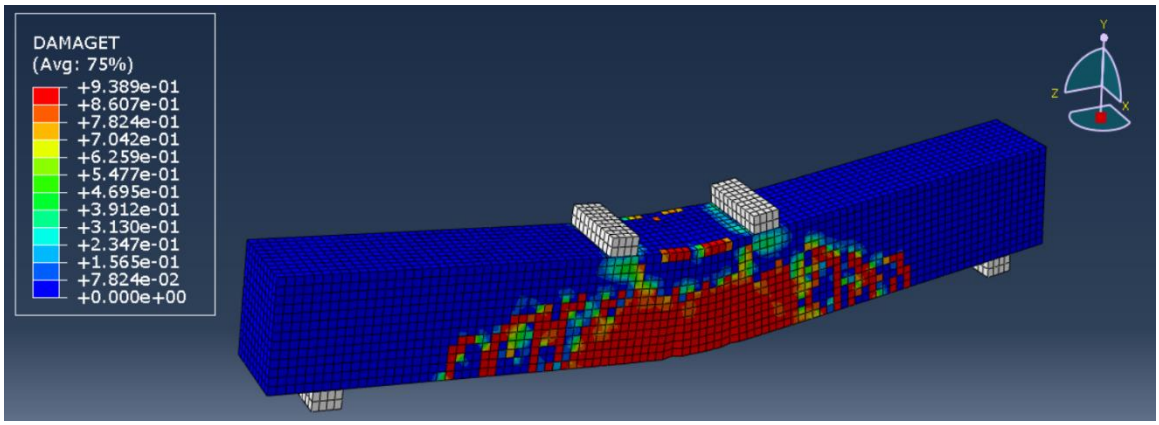

Picture 25: SMA-Phi16 Model - Tension Damage

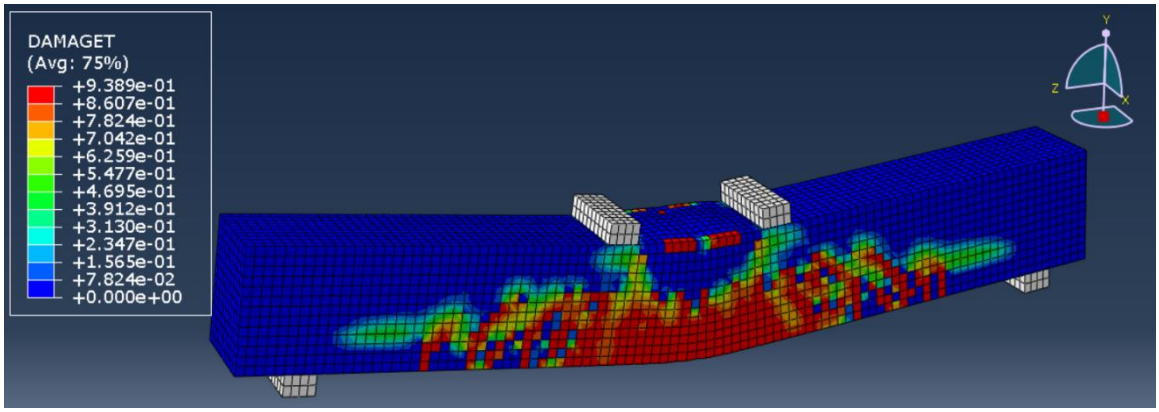

Picture 26: SMA-Phi18 Model - Tension Damage

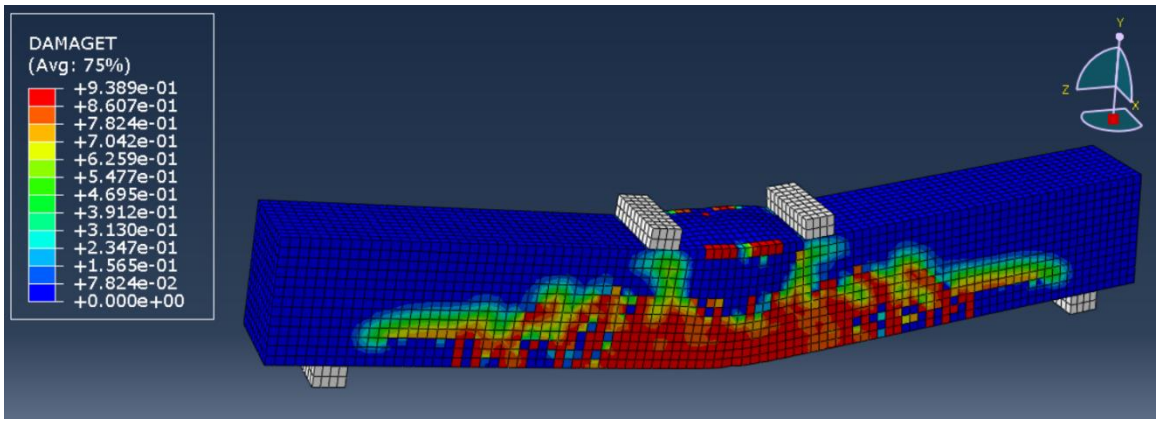

Picture 27: SMA-Phi22 Model - Tension Damage

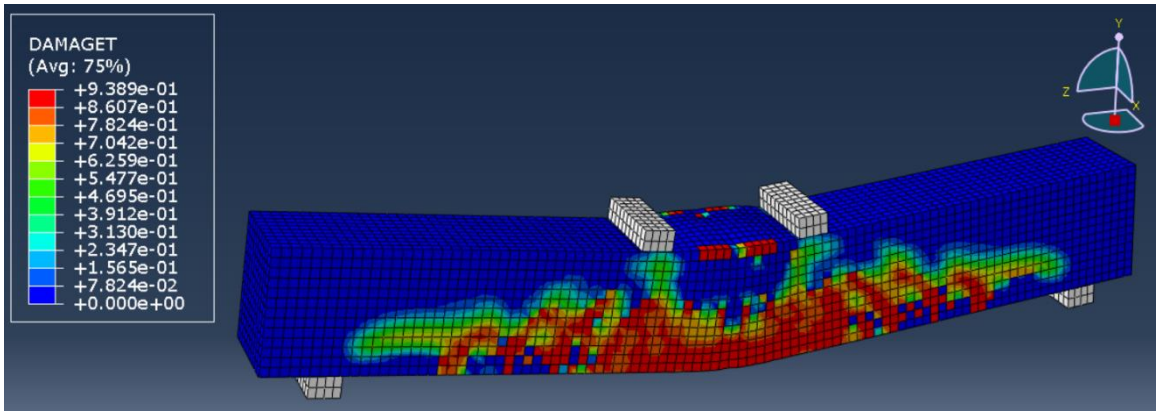

Picture 28: SMA-Phi24 Model - Tension Damage

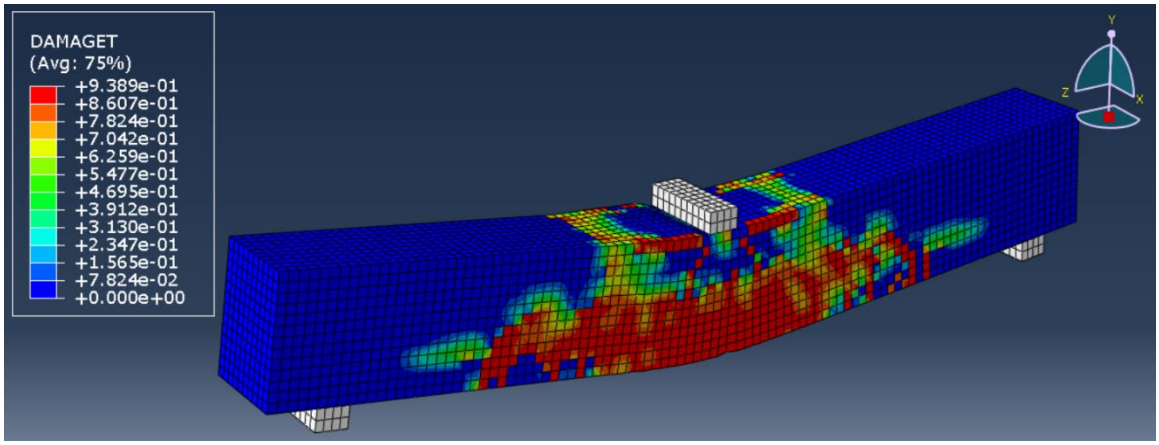

Picture 29: SMA-0 Model - Tension Damage

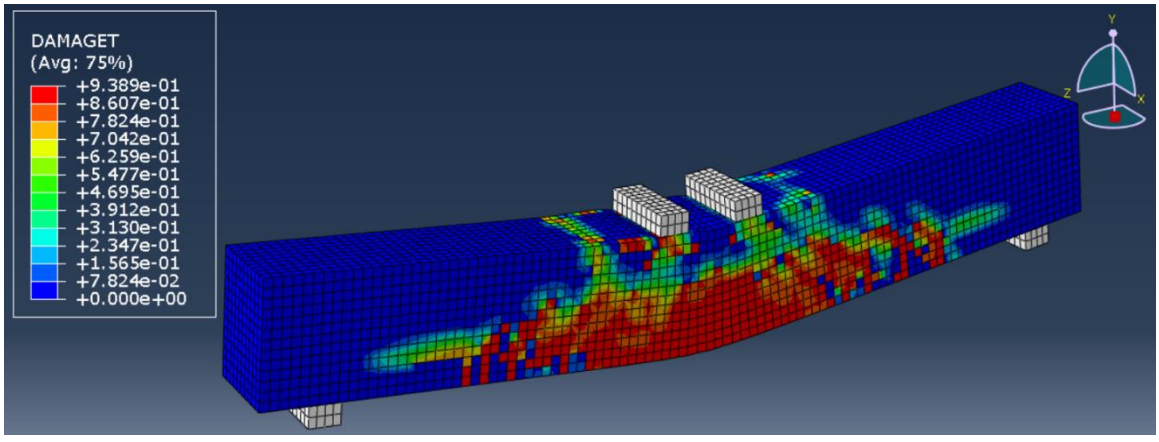

Picture 30: SMA-150 Model - Tension Damage

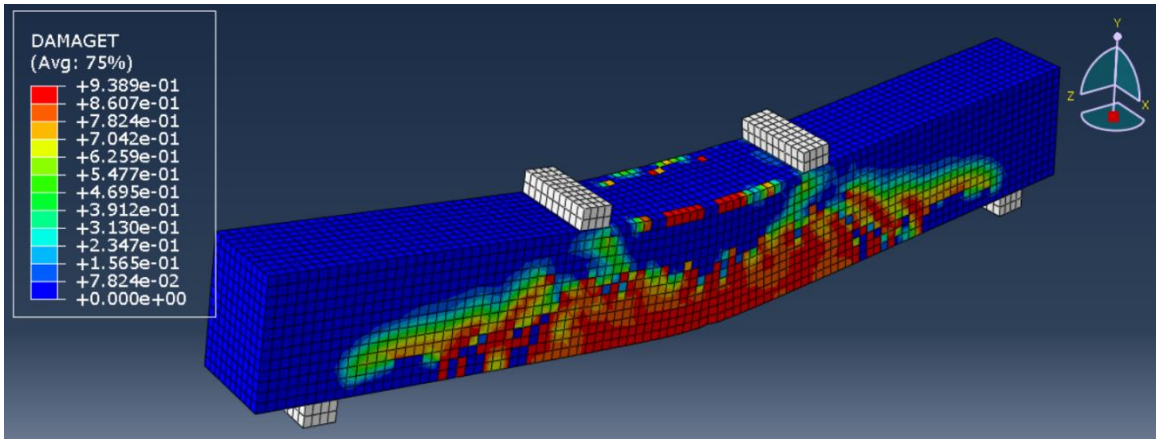

Picture 31: SMA-450 Model - Tension Damage

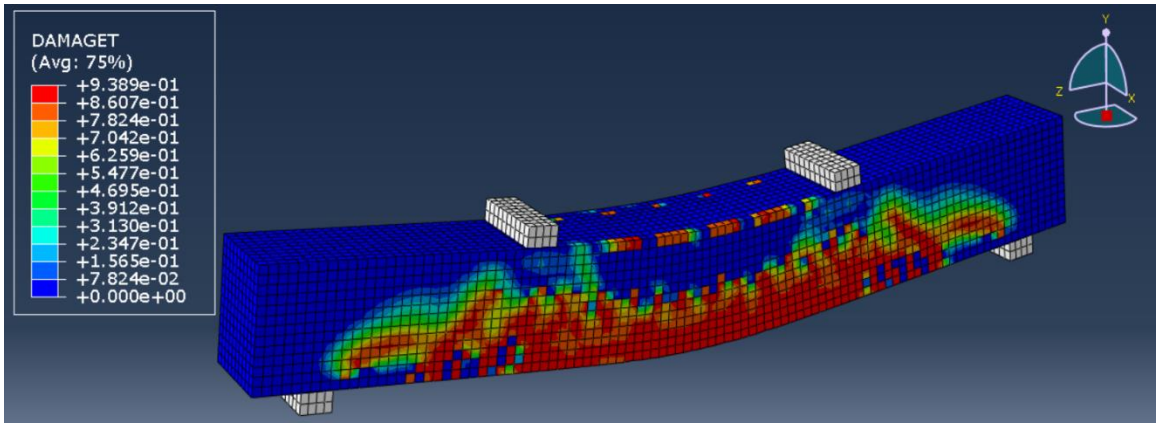

Picture 32: SMA-600 Model - Tension Damage

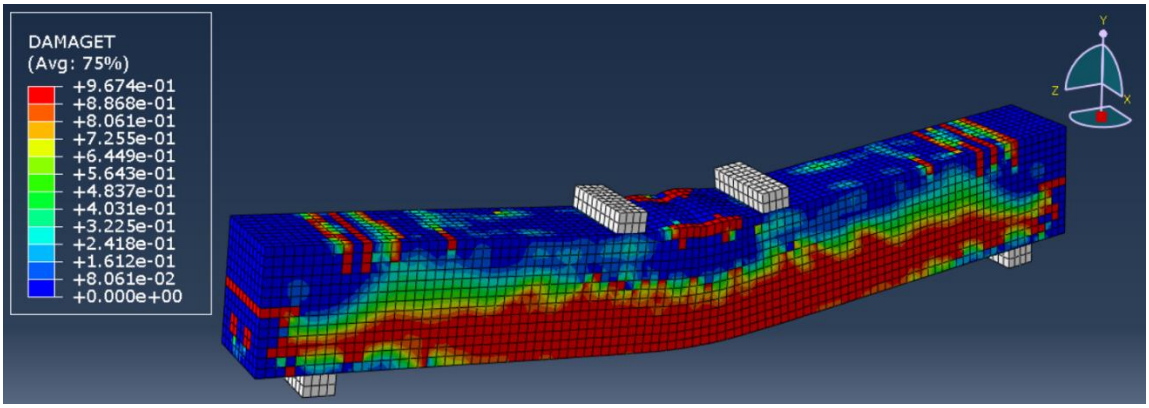

Picture 33: 20MPa-ConcreteModel - Tension Damage

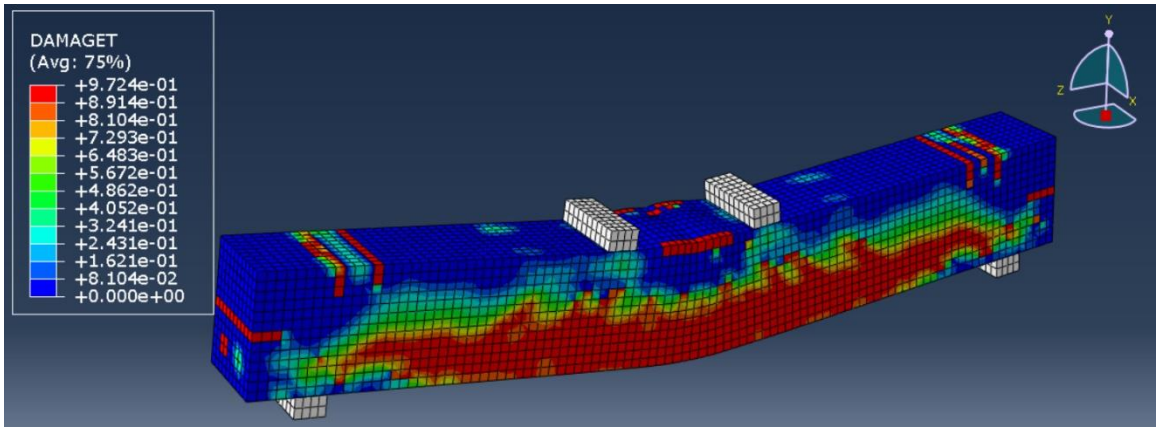

Picture 34: 28MPa-ConcreteModel - Tension Damage

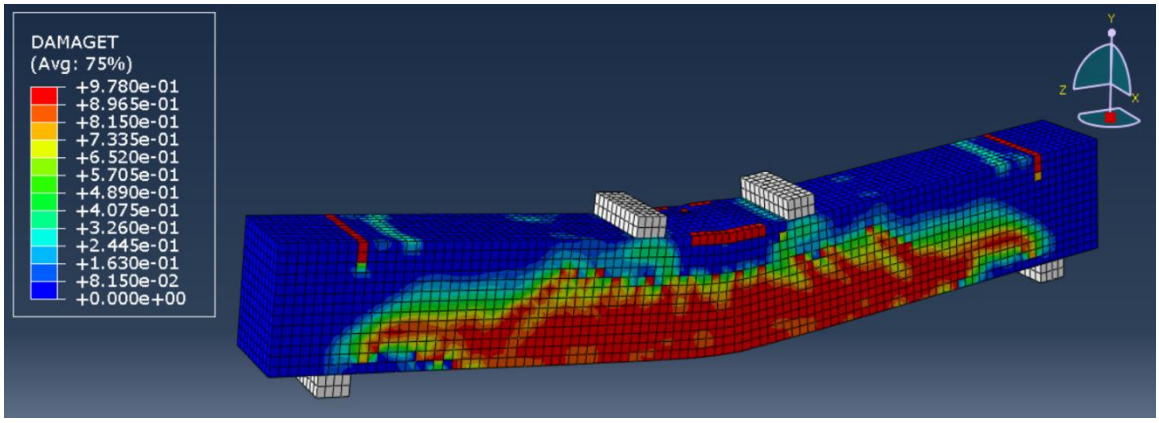

Picture 35: 44MPa-ConcreteModel - Tension Damage

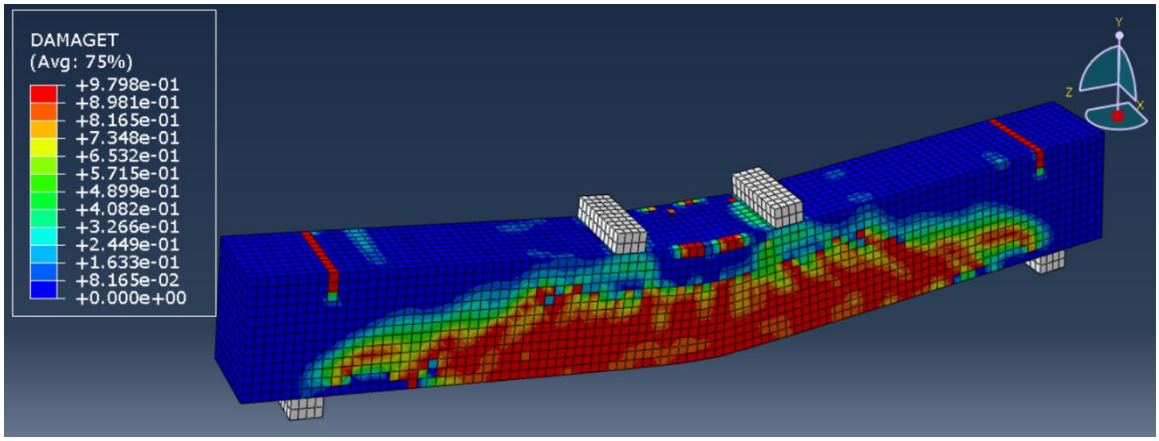

Picture 36: 52MPa-ConcreteModel - Tension Damage

5.2 Damage in compression

In this section, damagec (Compression Damage) will be shown for all models studied.

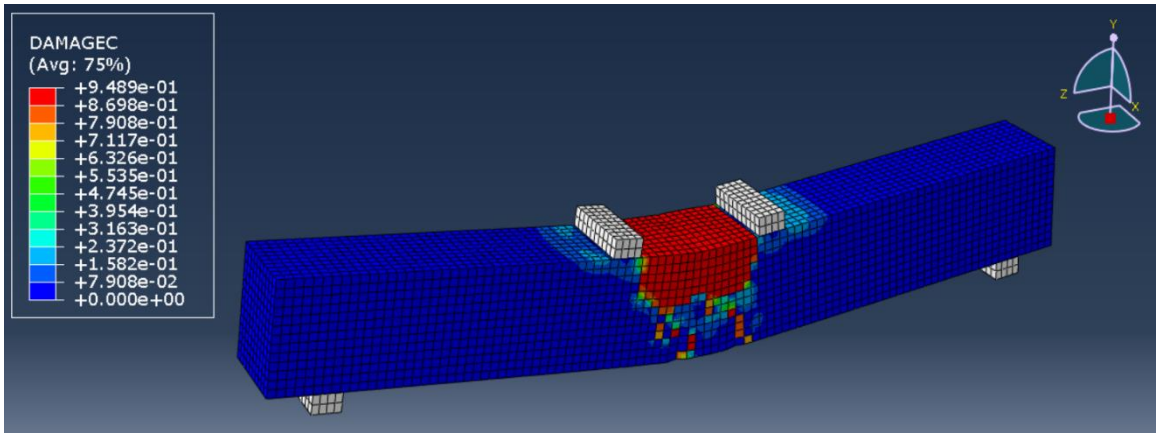

Picture 37: SMA-Phi16 Model - Compression Damage

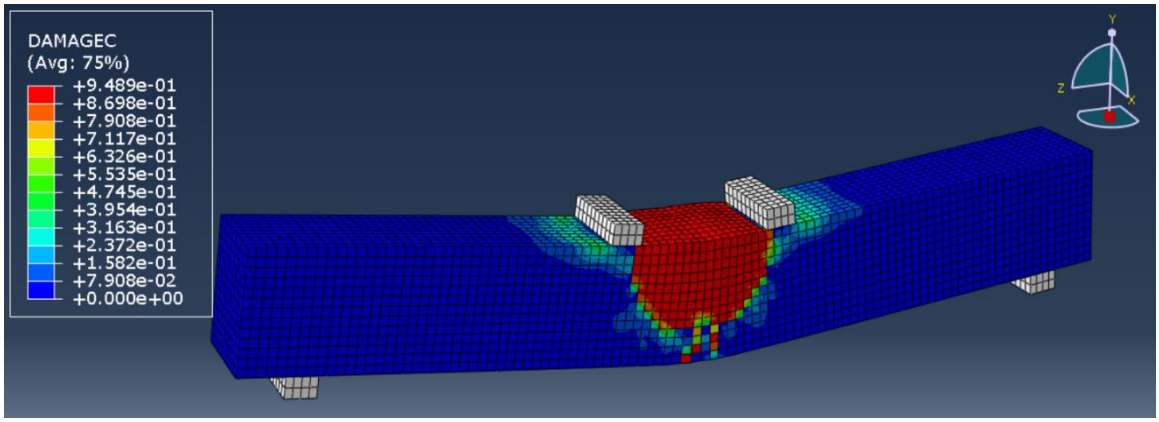

Picture 38: SMA-Phi18 Model - Compression Damage

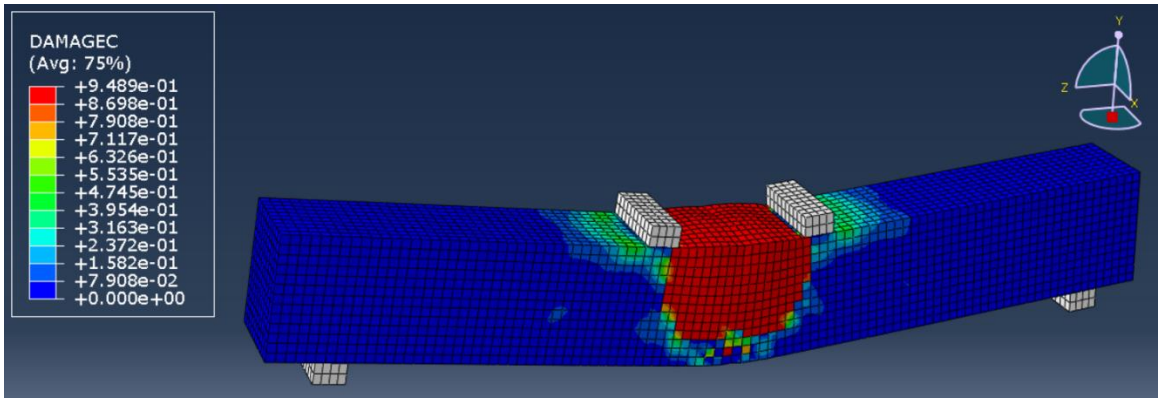

Picture 39: SMA-Phi22 Model - Compression Damage

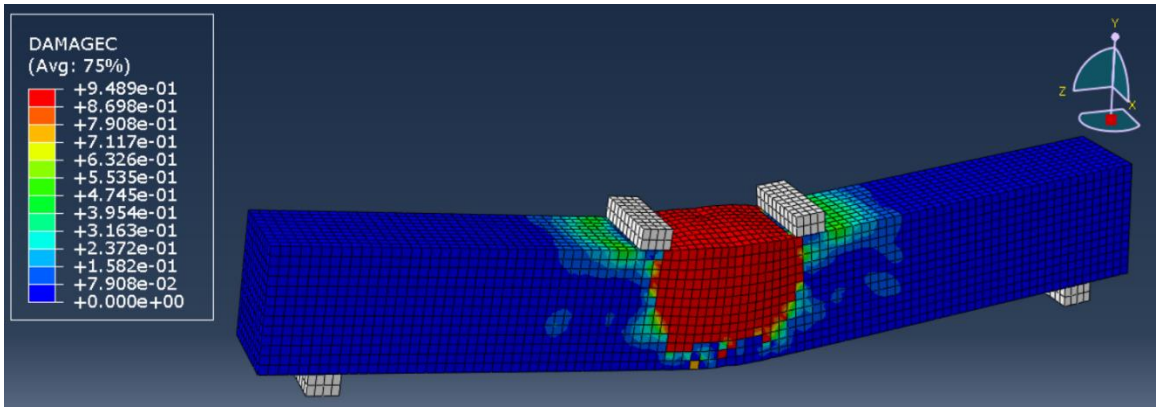

Picture 40: SMA-Phi24 Model - Compression Damage

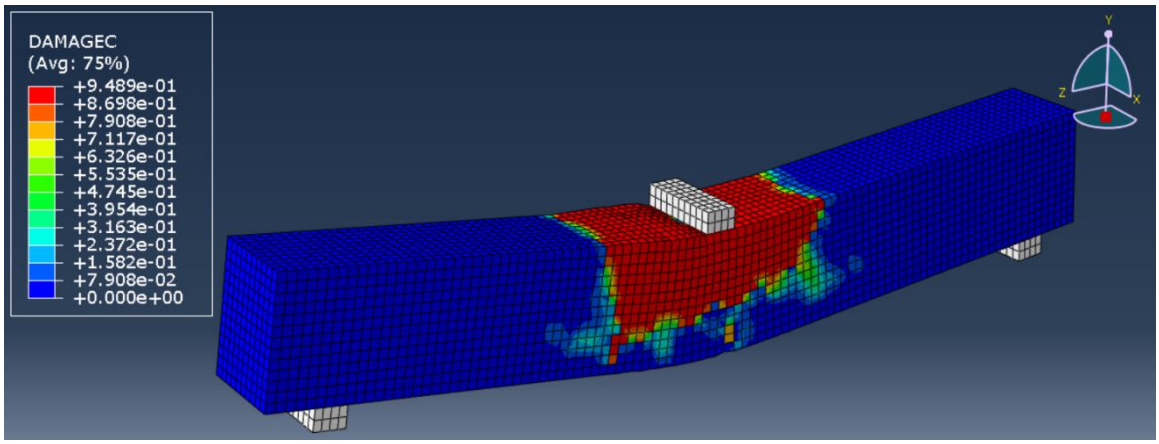

Picture 41: SMA-0 Model - Compression Damage

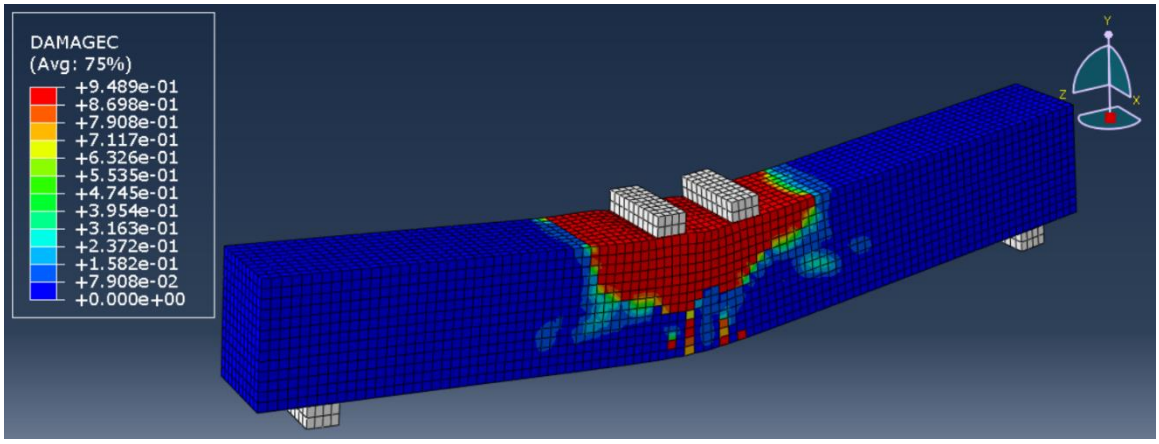

Picture 42: SMA-150 Model - Compression Damage

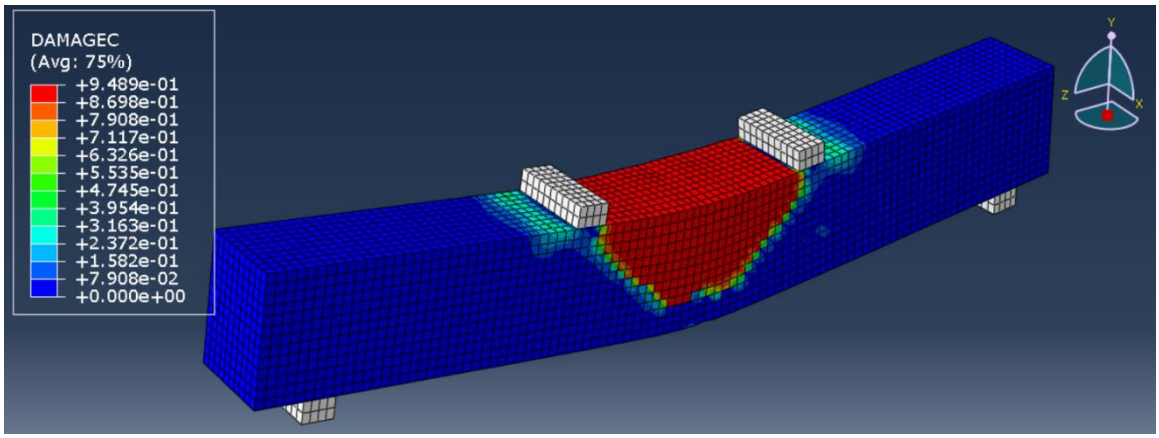

Picture 43: SMA-450 Model - Compression Damage

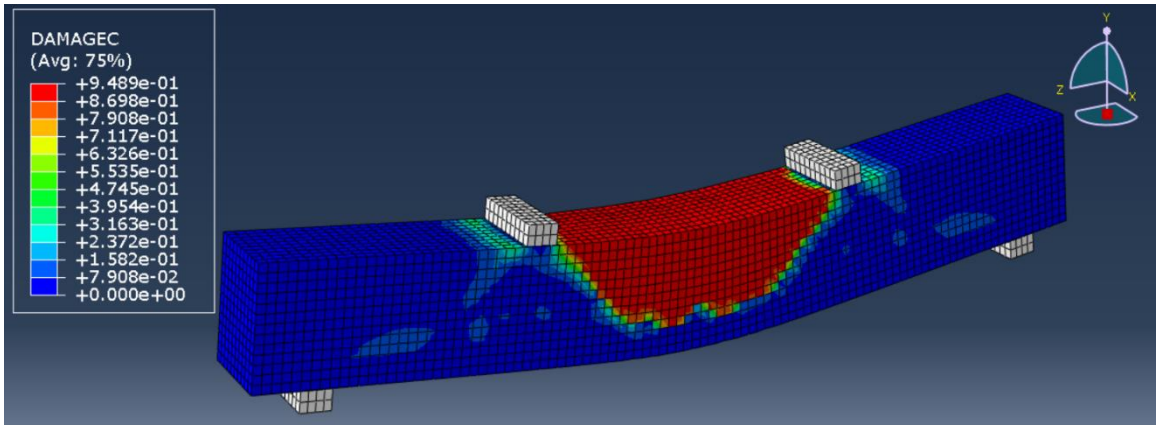

Picture 44: SMA-600 Model - Compression Damage

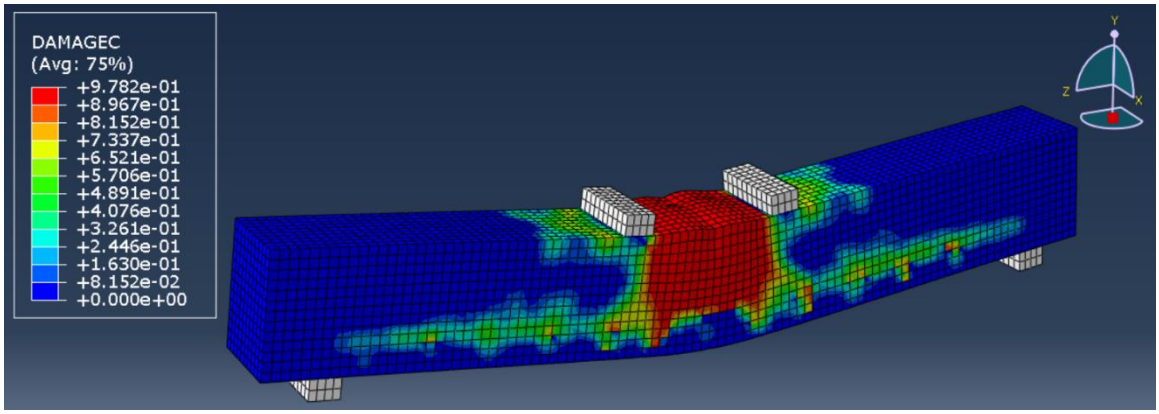

Picture 45: 20MPa-ConcreteModel - Compression Damage

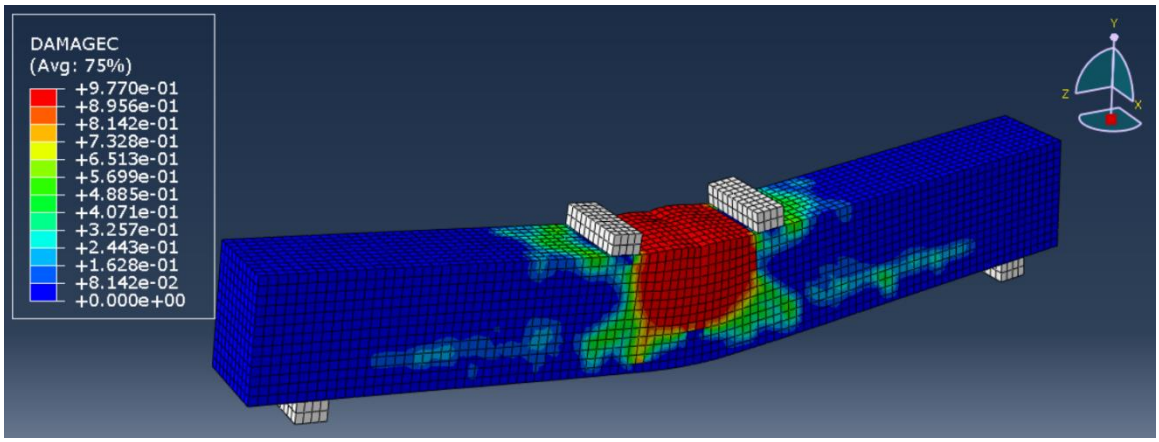

Picture 46: 28MPa-ConcreteModel - Compression Damage

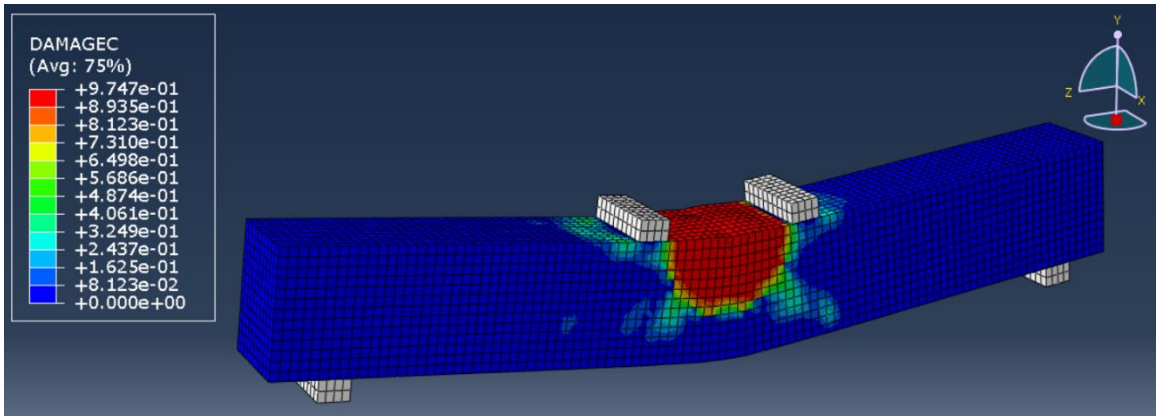

Picture 47: 44MPa-ConcreteModel - Compression Damage

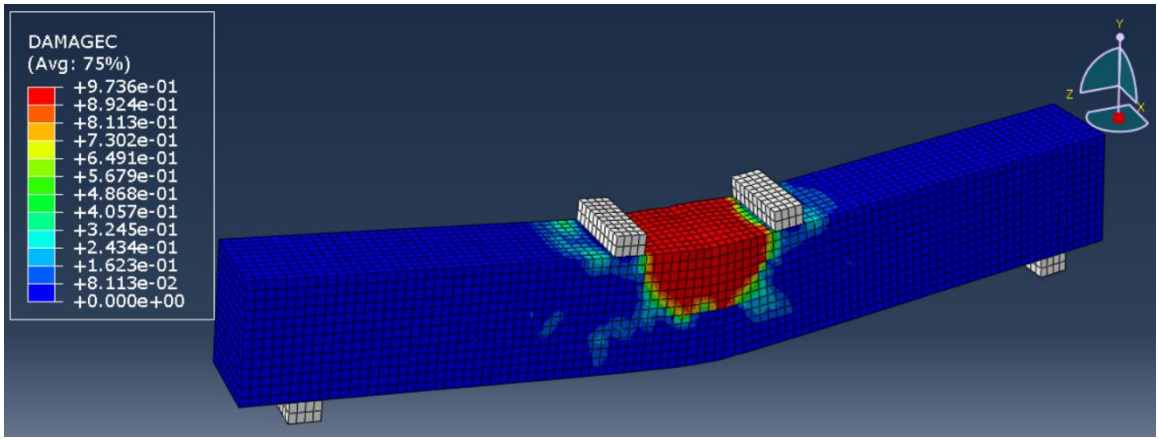

Picture 48: 52MPa-ConcreteModel - Compression Damage

5.3 Reinforcement normal stress

In this section, reinforcement normal stresses will be shown for all models studied.

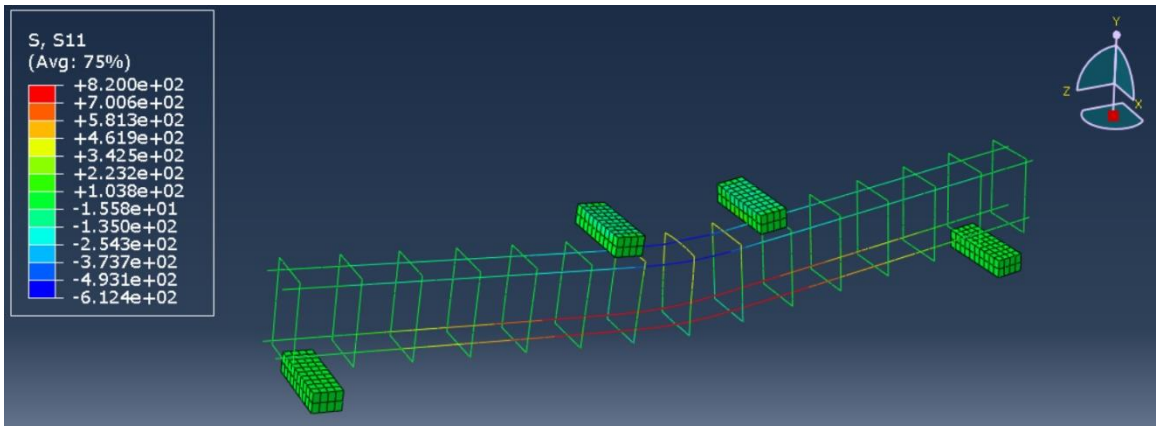

Picture 49: SMA-Phi16 Model - Reinforcement Normal Stress

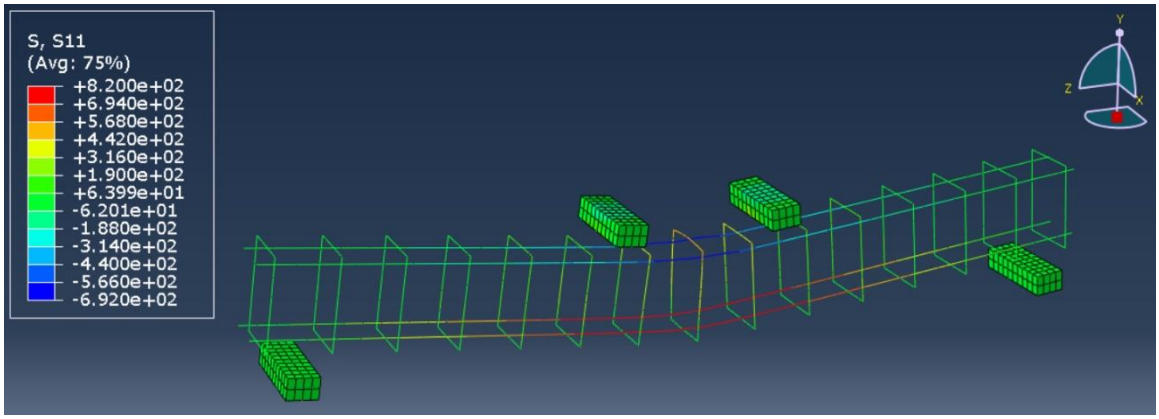

Picture 50: SMA-Phi18 Model - Reinforcement Normal Stress

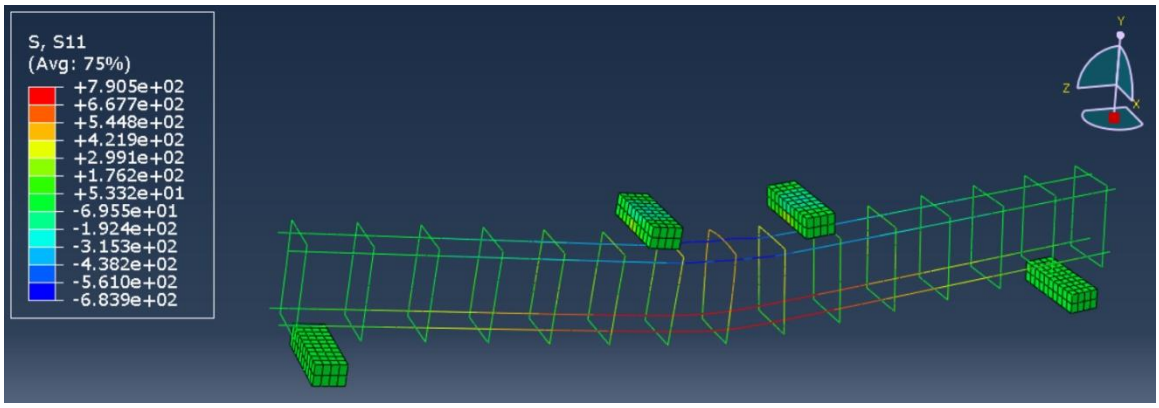

Picture 51: SMA-Phi22 Model - Reinforcement Normal Stress

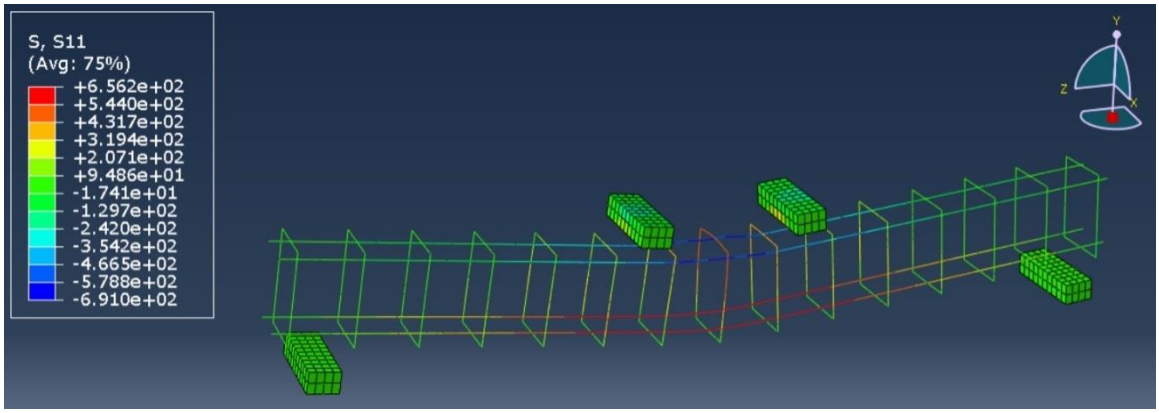

Picture 52: SMA-Phi24 Model - Reinforcement Normal Stress

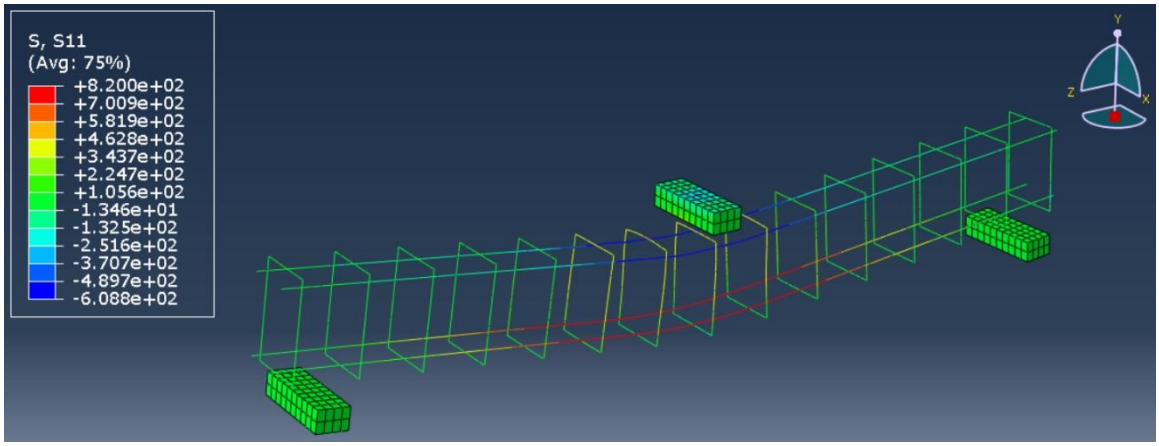

Picture 53: SMA-0 Model - Reinforcement Normal Stress

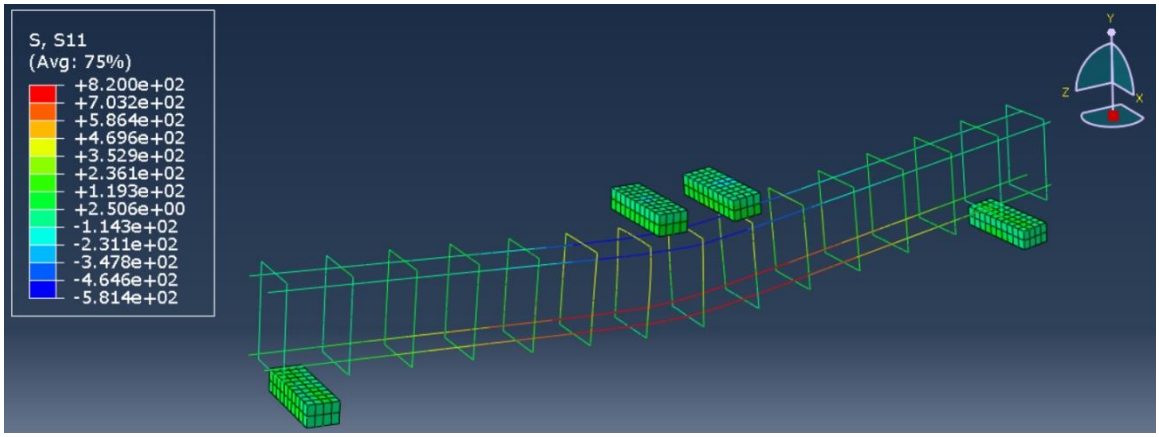

Picture 54: SMA-150 Model - Reinforcement Normal Stress

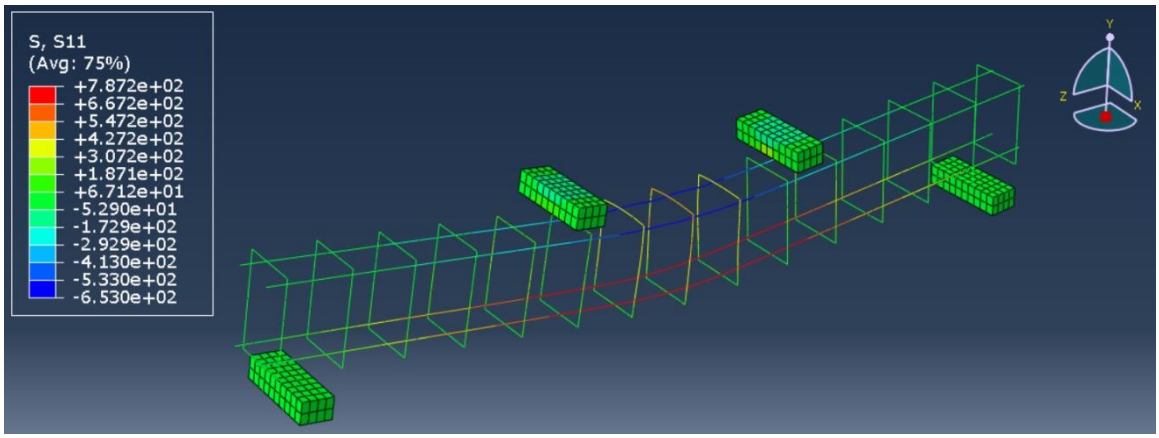

Picture 55: SMA-450 Model - Reinforcement Normal Stress

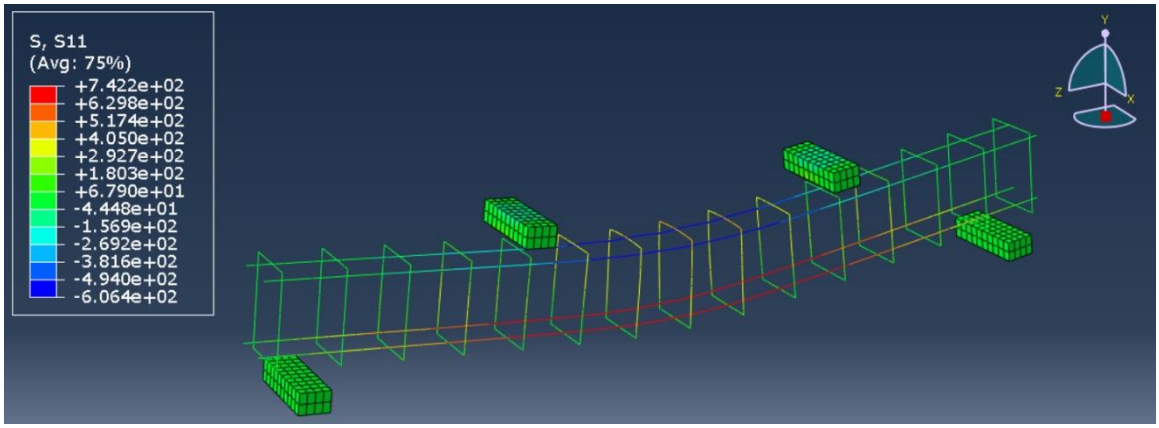

Picture 56: SMA-600 Model - Reinforcement Normal Stress

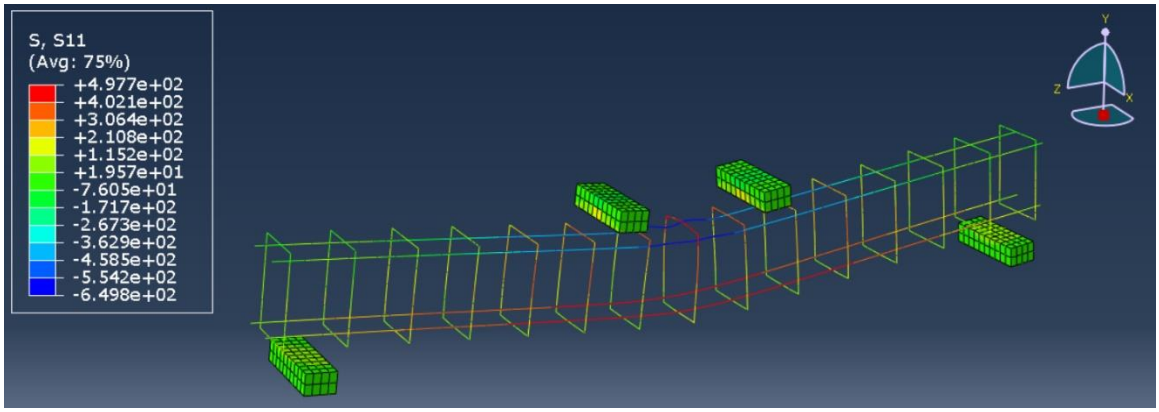

Picture 57: 20MPa-ConcreteModel - Reinforcement Normal Stress

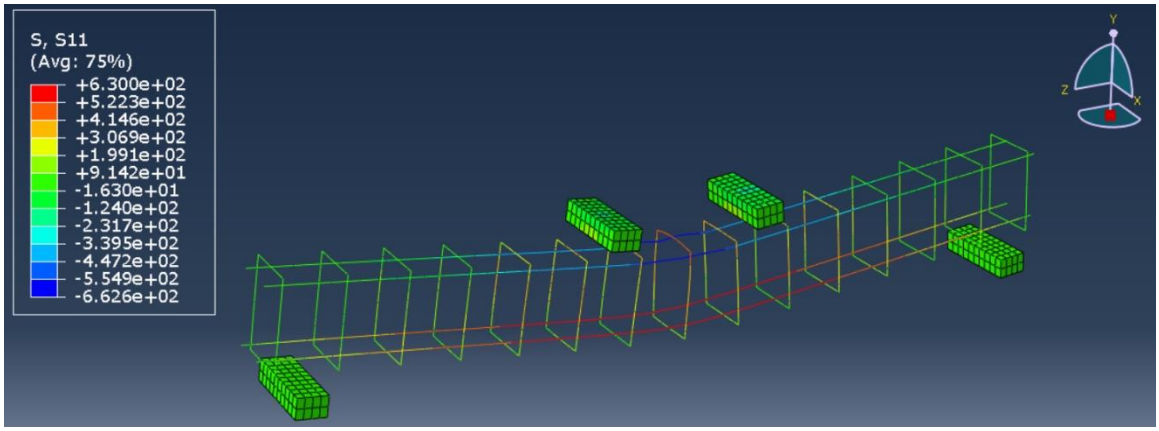

Picture 58: 28MPa-ConcreteModel - Reinforcement Normal Stress

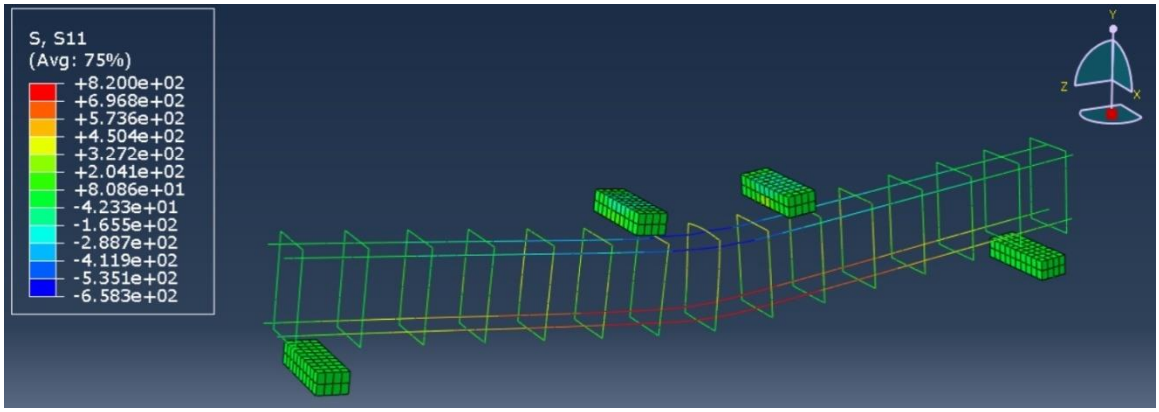

Picture 59: 44MPa-ConcreteModel - Reinforcement Normal Stress

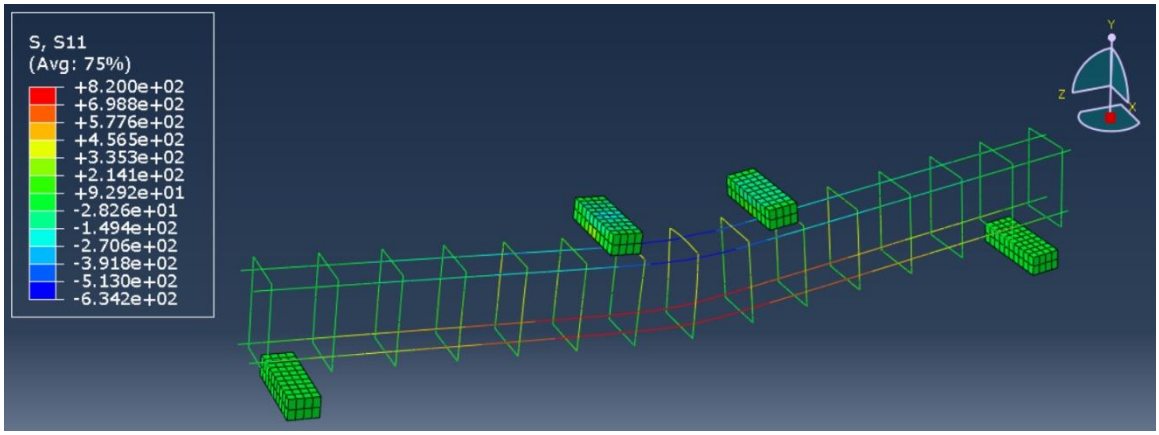

Picture 60: 52MPa-ConcreteModel - Reinforcement Normal Stress

5.4 Load-Displacement curve

In this section, load-displacement curves will be shown for all models studied.

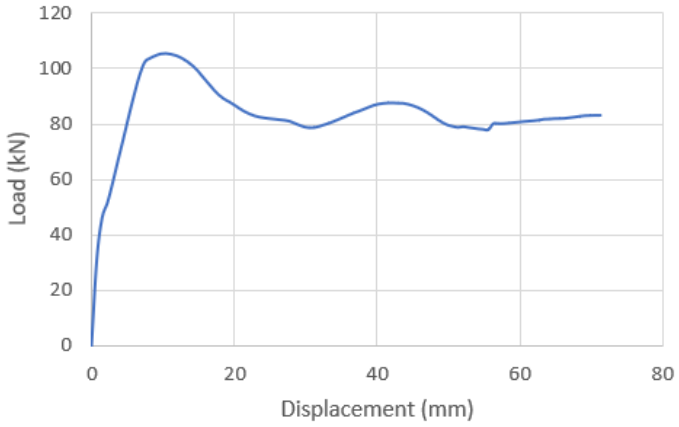

Figure 23: Load-Displacement curve for SMA-Phi16 Model

As can be seen in the figure above, the absolute maximum load capacity of 105.43 kN at a midspan displacement of 10.4 mm.

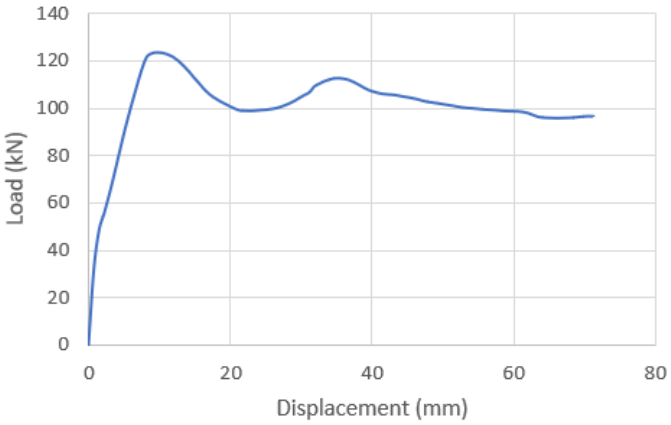

Figure 24: Load-Displacement curve for SMA-Phi18 Model

As can be seen in the figure above, the absolute maximum load capacity was 123.68 kN at a midspan displacement of 9.7 mm. And a local maximum load capacity of 112.81 kN at a midspan displacement of 35.3 mm.

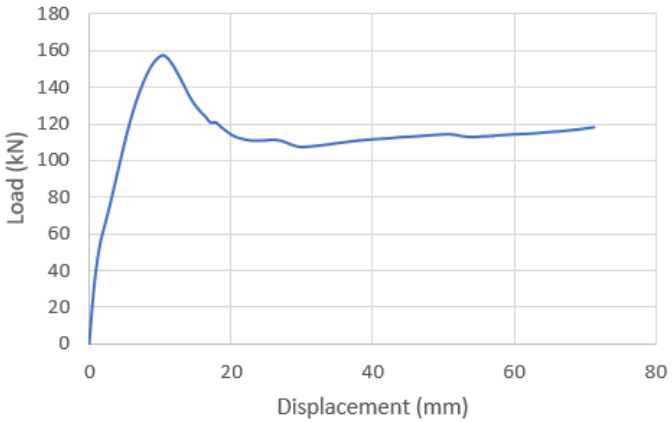

Figure 25: Load-Displacement curve for SMA-Phi22 Model

Based on the figure above, the maximum load capacity was 157.17 kN at a midspan displacement of 10.4 mm.

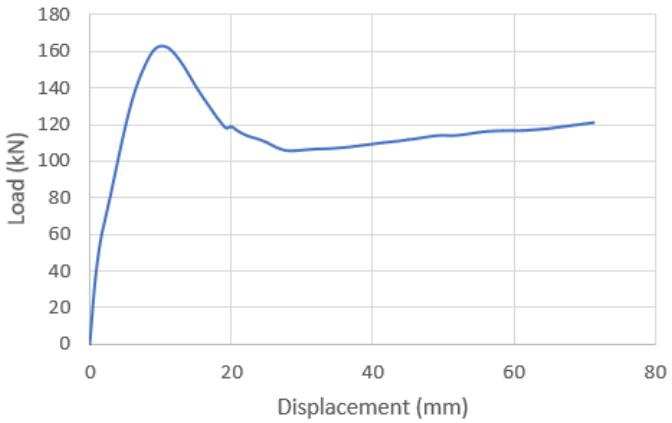

Figure 26: Load-Displacement curve for SMA-Phi24 Model

The figure above shows the maximum load capacity was 162.53 kN at a midspan displacement of 10.4 mm.

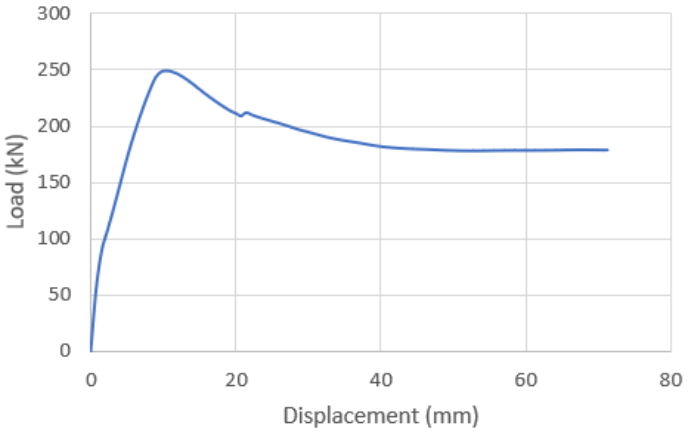

Figure 27: Load-Displacement curve for SMA-0 Model

As can be seen in the figure above, the maximum load capacity was 248.66 kN at a midspan displacement of 10.4 mm.

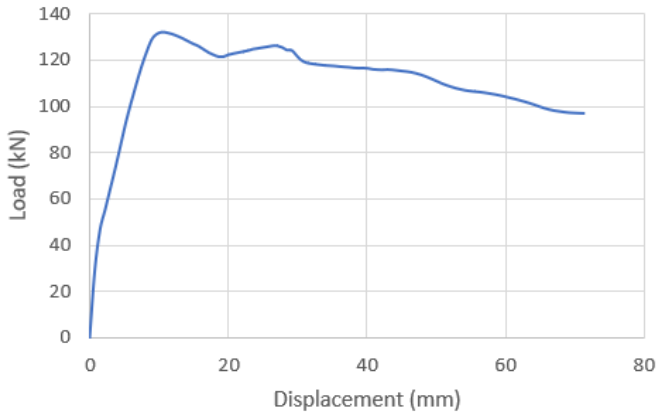

Figure 28: Load-Displacement curve for SMA-150 Model

As can be seen in the figure above, the absolute maximum load capacity was 131.9 kN at a midspan displacement of 10.4 mm. And a local maximum load capacity of 126 kN at a midspan displacement of 27 mm.

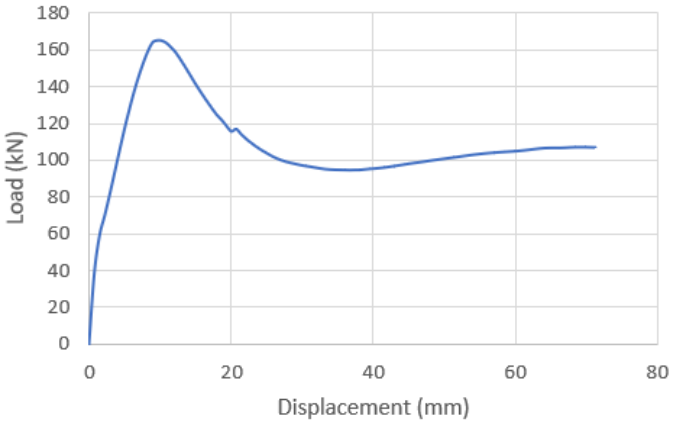

Figure 29: Load-Displacement curve for SMA-450 Model

As shown in the figure above, the maximum load capacity was 164.87 kN at a midspan displacement of 9.7 mm.

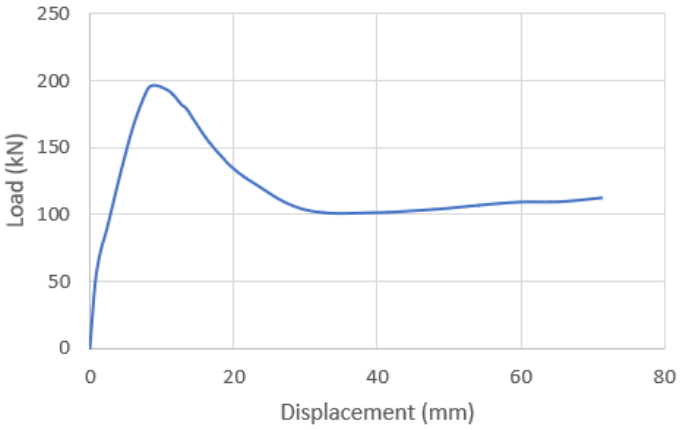

Figure 30: Load-Displacement curve for SMA-600 Model

As presented in the figure above, the maximum load capacity was 196.8 kN at a midspan displacement of 9 mm.

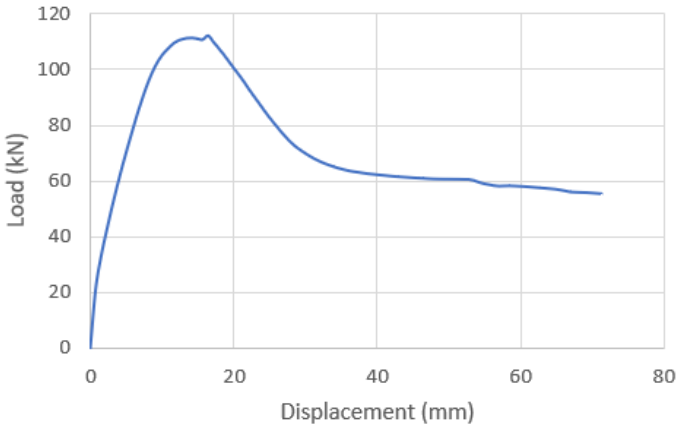

Figure 31: Load-Displacement curve for 20MPa-ConcreteModel

As presented in the figure above, the maximum load capacity was 111.23 kN at a midspan displacement of 14.2 mm.

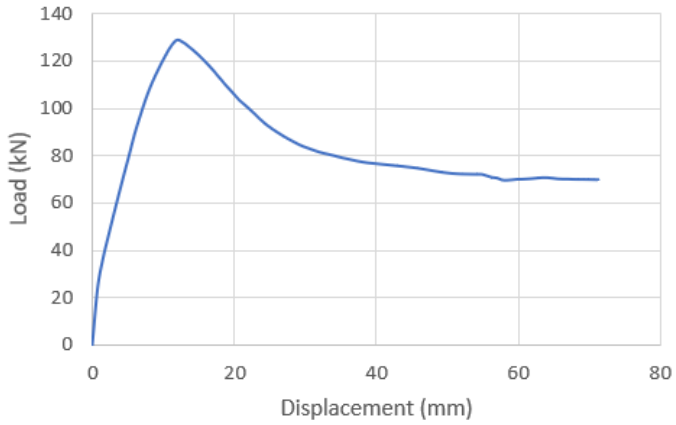

Figure 32: Load-Displacement curve for 28MPa-ConcreteModel

As presented in the figure above, the maximum load capacity was 129.23 kN at a midspan displacement of 11.9 mm.

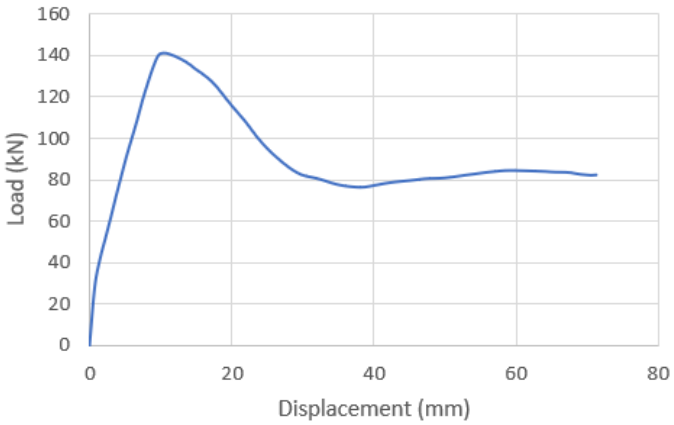

Figure 33: Load-Displacement curve for 44MPa-ConcreteModel

As presented in the figure above, the maximum load capacity was 141.05 kN at a midspan displacement of 10.4 mm.

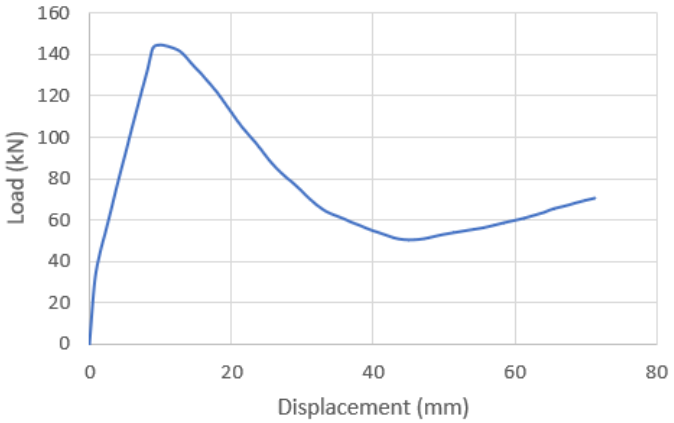

Figure 34: Load-Displacement curve for 52MPa-ConcreteModel

As presented in the figure above, the maximum load capacity was 144.79 kN at a midspan displacement of 9.7 mm.

5.5 Groups Load-Displacement curves

5.5.1 Changing the area of SMA bars

The SMA bars applied for resisting tension force were having different sizes as following:

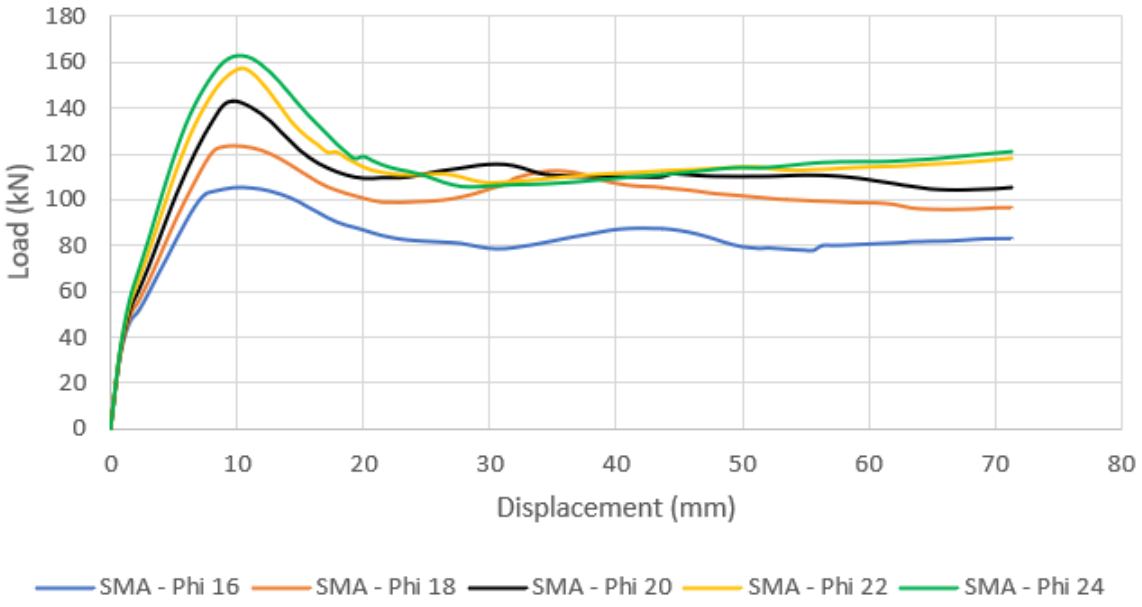

Figure 35: Load-Displacement Curves for Different SMA Bars' sizes

As can be noticed in the figure above, when increasing the SMA bar's area, a higher value for the maximum load capacity is obtained while maintaining this capacity at a displacement from 9.5 to 11 mm.

5.5.2 Changing distances between Loads

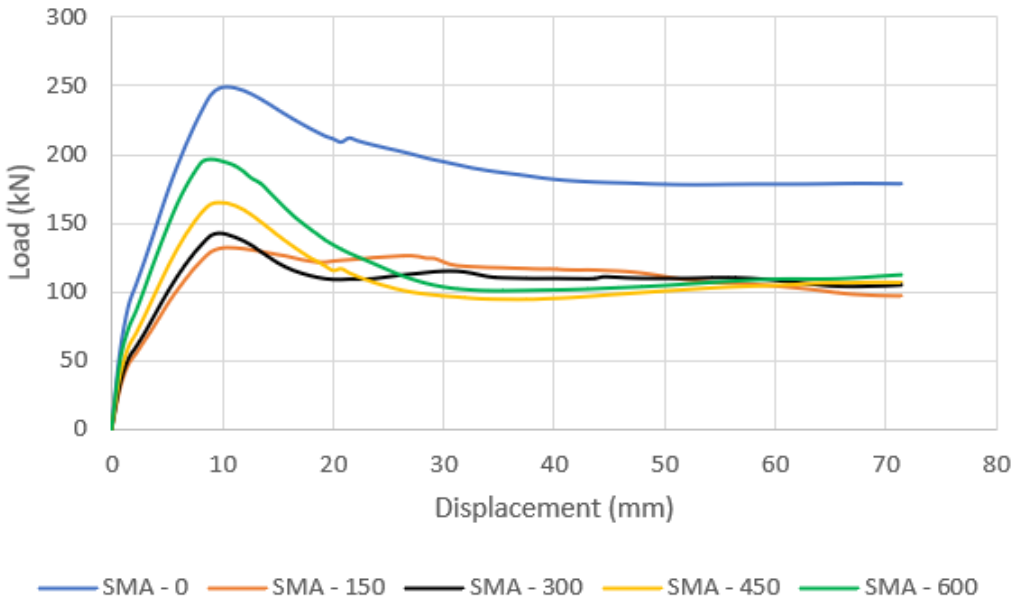

Figure 36: Load-Displacement Curves for Different Distances between Point Loads

As illustrated in the figure above, applying one load point on the beam will result in a noticeable high load capacity can be resisted. For the case of applying two-point loads, increasing the distance between these two points results in increasing the load capacity.

5.5.3Changing concrete compressive strength (fc`)

The SMA bars and loads applied on beams having different compressive strength as following:

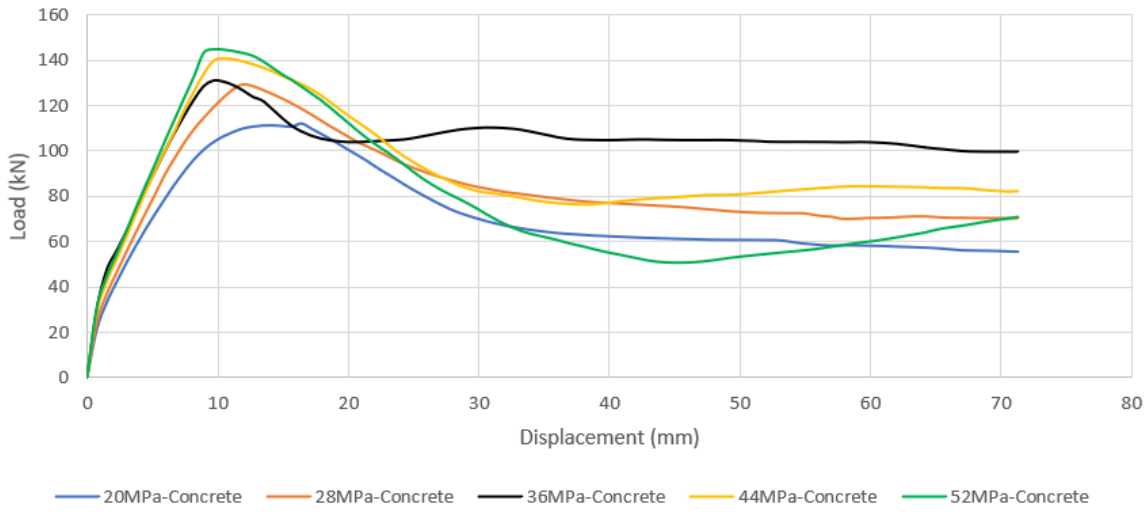

Figure 37: Load-Displacement Curves for Different Concrete Compressive Strength

As shown above, the maximum load strength is about 144.79 kN at the midspan displacement of 9.4 mm approximately in 52 MPa concrete. And near that for 44MPa but less than the first one. 28 and 36 MPa concrete showed an approximate load capacity. However, 36 MPa concrete can maintain the load capacity for further displacement.

5.5.4 Whole study

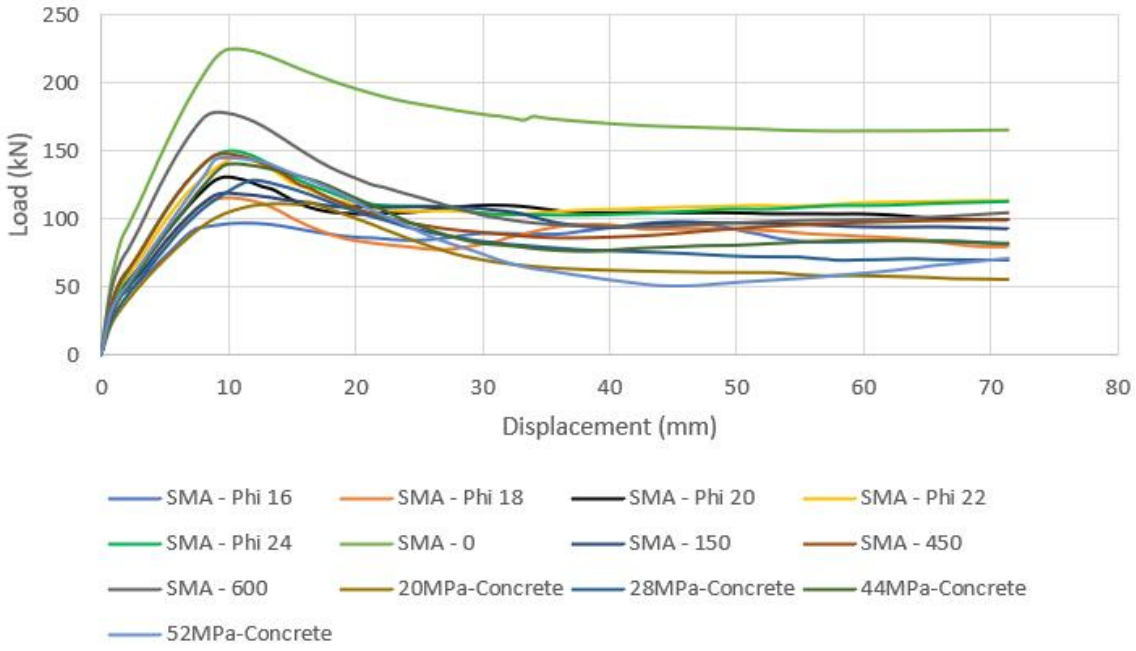

Figure 38: Load-Displacement Curves for all models

Comparing the results for fixing the SMA bars to phi 16 and changing the distance between loads with the results got from fixing the distance between loads to 300 mm and changing the SMA bars' areas, it can be concluded that the most two load capacities were obtained from fixing the SMAs' area with changing the distance between loads to 0 mm - only one point load applied- and 600 mm respectively. Then, the results were obtained are very close with keeping decreasing in load capacity. The least load capacity obtained from fixing the distance between loads to 300 mm and changing the SMA bars to Phi16.

Chapter 6: Conclusion

From models and figures in previous chapters, this study can be concluded in the following points:

- SMA can be used in place of steel tension reinforcement to increase strength.
- The load capacity is directly inversely related to the SMA reinforcement percentage (SMA diameter).
- In comparison to applying a two-point load, putting a single point load in the center of the beam increases the beam's load strength.
- When the distance between the two load locations was increased, the load strength of the beam increased.
- SMA is preferred to be used when the concrete has higher compressive strength. The benefits of employing SMA may disappear if the concrete has a low compressive strength.

Chapter 7: References

Choi, E., Nam, T., Cho, S.-C., Chung, Y.-S., Park, T., 2008. The behavior of concrete cylinders confined by shape memory alloy wires. Smart Materials and Structures 17, 065032.

Cladera, A., Weber, B., Leinenbach, C., Czaderski, C., Shahverdi, M., Motavalli, M., 2014. Iron-based shape memory alloys for civil engineering structures: An overview. Construction and building materials 63, 281–293.

Czaderski, C., Hahnebach, B., Motavalli, M., 2006. RC beam with variable stiffness and strength. Construction and building materials 20, 824–833.

Deng, Z., Li, Q., Sun, H., 2006. Behavior of concrete beam with embedded shape memory alloy wires. Engineering Structures 28, 1691–1697. https://doi.org/10.1016/j.engstruct.2006.03.002

Dolce, M., Cardone, D., 2001. Mechanical behaviour of shape memory alloys for seismic applications 2. Austenite NiTi wires subjected to tension. International journal of mechanical sciences 43, 2657–2677.

Dommer, K., Andrawes, B., 2012. Thermomechanical characterization of NiTiNb shape memory alloy for concrete active confinement applications. Journal of Materials in Civil Engineering 24, 1274–1282.

El-Tawil, S., Ortega-Rosales, J., 2004. Prestressing concrete using shape memory alloy tendons. Structural Journal 101, 846–851.

Gibert, J.M.R., 2019. Active shear strengthening of reinforced concrete beams using Ni-Ti-Nb shape memory alloys.

Granito_Michele_23.pdf,2010.

Hsu, D.H.D., 2013 DESIGN AND DEVELOPMENT OF NiTi-BASED PRECIPITATION-STRENGTHENED HIGH-TEMPERATURE SHAPE MEMORY ALLOYS FOR ACTUATOR APPLICATIONS 148.

Janke, L., 2005. Applications of shape memory alloys in civil engineering structures - Overview, limits and new ideas. Mater. Struct. 38, 578–592. https://doi.org/10.1617/14323

Karimipour, A., Edalati, M., 2020. RETRACTED: Shear and flexural performance of low, normal and high-strength concrete beams reinforced with longitudinal SMA, GFRP

and steel rebars. Engineering Structures 221, 111086. https://doi.org/10.1016/j.engstruct.2020.111086

Lee, W., Weber, B., Feltrin, G., Czaderski, C., Motavalli, M., Leinenbach, C., 2013. Phase transformation behavior under uniaxial deformation of an Fe–Mn–Si–Cr–Ni–VC shape memory alloy. Materials Science and Engineering: A 581, 1–7.

Lee, W.J., Weber, B., Leinenbach, C., 2015. Recovery stress formation in a restrained Fe–Mn–Si-based shape memory alloy used for prestressing or mechanical joining. Construction and Building Materials 95, 600–610. https://doi.org/10.1016/j.conbuildmat.2015.07.098

Leinenbach, C., Kramer, H., Bernhard, C., Eifler, D., 2012. Thermo-Mechanical Properties of an Fe–Mn–Si–Cr–Ni–VC Shape Memory Alloy with Low Transformation Temperature. Advanced Engineering Materials 14, 62–67.

Maji, A.K., Negret, I., 1998. Smart prestressing with shape-memory alloy. Journal of engineering mechanics 124, 1121–1128.

Mas, B., Biggs, D., Vieito, I., Cladera, A., Shaw, J., Martínez-Abella, F., 2017. Superelastic shape memory alloy cables for reinforced concrete applications. Construction and Building Materials 148, 307–320. https://doi.org/10.1016/j.conbuildmat.2017.05.041

Mas, B., Cladera, A., Ribas, C., 2016. Fundamentals and pilot experiences of the application of shape memory alloys in structural engineering. Hormigón y Acero 67, 309–323.

Rojob, H., El-Hacha, R.,2017 New anchorage mechanism for smooth Fe-SMA bar used for flexural strengthening of RC beams using NSM technique 8.

Shahverdi, M., Czaderski, C., Motavalli, M., 2016. Iron-based shape memory alloys for prestressed near-surface mounted strengthening of reinforced concrete beams. Construction and Building Materials 112, 28–38. https://doi.org/10.1016/j.conbuildmat.2016.02.174

Shin, M., Andrawes, B., 2012. Modeling and Validation of RC Columns Seismically Retrofitted Using Shape Memory Spiral, in: Structures Congress 2012. Presented at the Structures Congress 2012, American Society of Civil Engineers, Chicago, Illinois, United States, pp. 571–580. https://doi.org/10.1061/9780784412367.051

Shin, M., Andrawes, B., 2010. Experimental investigation of actively confined concrete using shape memory alloys. Engineering Structures 32, 656–664.

Song, G., Ma, N., Li, H.-N., 2006. Applications of shape memory alloys in civil structures. Engineering Structures 28, 1266–1274. https://doi.org/10.1016/j.engstruct.2005.12.010

Soroushian, P., Ostowari, K., Nossoni, A., Chowdhury, H., 2001. Repair and strengthening of concrete structures through application of corrective posttensioning forces with shape memory alloys. Transportation Research Record 1770, 20–26.

Asran, G., El-Esnawi, H., Fayed, S., 2016. Numerical investigation of RC exterior beam colum connections under monotonic loads. Journal of Mechanical and Civil Engineering 13, 60–67.

Ghobarah, A., Said, A., 2002. Shear strengthening of beam-column joints. Engineering structures 24, 881–888.

Karimipour, A., Edalati, M., 2020. RETRACTED: Shear and flexural performance of low, normal and high-strength concrete beams reinforced with longitudinal SMA, GFRP and steel rebars. Engineering Structures 221, 111086. https://doi.org/10.1016/j.engstruct.2020.111086

Kmiecik, P., Kamiński, M., 2011. Modelling of reinforced concrete structures and composite structures with concrete strength degradation taken into consideration. Archives of civil and mechanical engineering 11, 623–636.

Lee, J., Fenves, G.L., 1998. Plastic-damage model for cyclic loading of concrete structures. Journal of engineering mechanics 124, 892–900.

Mander, J.B., Priestley, M.J., Park, R., 1988. Theoretical stress-strain model for confined concrete. Journal of structural engineering 114, 1804–1826.

Pereiro-Barceló, J., Bonet, J.L., Albiol-Ibáñez, J.R., 2018. Buckling of steel and Ni-Ti reinforcements in very high performance concrete (VHPC) elements. Construction and Building Materials 160, 551–563.

Saenz, L.P., 1964. discussion of" Equation for the Stress-Strain Curve of Concrete" by Desayi and Krishnan. Journal of the American Concrete Institute 61, 1229–1235.

Sharif, A.M., Samaaneh, M.A., Azad, A.K., Baluch, M.H., 2016. Use of CFRP to maintain composite action for continuous steel–concrete composite girders. Journal of Composites for Construction 20, 04015088.

Simulia, D.S., 2013. ABAQUS 6.13 User’s manual. Dassault Systems, Providence, RI 305, 306.

Viet, N., Zaki, W., 2019. Analytical investigation of the behavior of concrete beams reinforced with multiple circular superelastic shape memory alloy bars. Composite Structures 210, 958–970.

Wahalathantri, B., Thambiratnam, D., Chan, T., Fawzia, S., 2011. A material model for flexural crack simulation in reinforced concrete elements using ABAQUS. Presented at the Proceedings of the first international conference on engineering, designing and developing the built environment for sustainable wellbeing, Queensland University of Technology, pp. 260–264.

Willam, K., Warnke, E., 1975. Constitutive Model for the Triaxial Behavior of Concrete. International Association for Bridge and Structural Engineering. Presented at the Proceedings.

Yong, Y.-K., Nour, M.G., Nawy, E.G., 1988. Behavior of laterally confined high-strength concrete under axial loads. Journal of Structural Engineering 114, 332–351.